Published for SISSA by Springer

Received: May 26, 2023
Revised: July 4, 2023
Accepted: July 16, 2023
Published: August 22, 2023

Holographic CFT phase transitions and criticality for rotating AdS black holes

Moaathe Belhaj Ahmed,[a] **Wan Cong,**[b] **David Kubizňák,**[c,d] **Robert B. Mann**[a,d] **and Manus R. Visser**[e]

[a] *Department of Physics and Astronomy, University of Waterloo, Waterloo, Ontario, N2L 3G1, Canada*
[b] *Faculty of Physics, University of Vienna, Vienna, Austria*
[c] *Institute of Theoretical Physics, Faculty of Mathematics and Physics, Charles University, V Holešovičkách 2, 180 00 Prague 8, Czech Republic*
[d] *Perimeter Institute for Theoretical Physics, 31 Caroline St., Waterloo, Ontario, N2L 2Y5, Canada*
[e] *Department of Applied Mathematics and Theoretical Physics, University of Cambridge, Wilberforce Road, Cambridge CB3 0WA, United Kingdom*

E-mail: hoothyy789@gmail.com, wan.cong@univie.ac.at, david.kubiznak@matfyz.cuni.cz, rbmann@uwaterloo.ca, mv551@cam.ac.uk

Abstract: Employing the novel exact dictionary between the laws of extended black hole thermodynamics and the laws of the dual CFT, we study the extended thermodynamics for CFT states that are dual to neutral singly-spinning asymptotically AdS black holes in d bulk spacetime dimensions. On the field theory side we include two independent pairs of thermodynamic conjugate variables: the central charge-chemical potential term and the pressure-volume term. In this setting we uncover various phase transitions and critical behaviour in the CFT, focusing on three different thermodynamic ensembles. Namely, for fixed angular momentum and central charge, we show there is a Van der Waals-like criticality for $d = 4, 5$ and reentrant phase transitions for $d \geq 6$. At fixed angular velocity and central charge, there is a first-order (de)confinement phase transition in all dimensions $d \geq 3$. Finally, at fixed angular momentum and chemical potential we find a plethora of zero-order phase transitions and unstable phases in both $d = 4$ and $d = 6$.

Keywords: AdS-CFT Correspondence, Black Holes

ArXiv ePrint: 2305.03161

https://doi.org/10.1007/JHEP08(2023)142

JHEP08(2023)142

Contents

JHEP08(2023)142

1 Introduction

One of the main advantages of holographic duality is that puzzling features of black holes can be studied in the dual field theory, and vice versa. The best understood example of such a duality is the AdS/CFT correspondence [1–3], where Anti-de Sitter (AdS) black holes have been argued to be equivalent to thermal states in the dual conformal field theory (CFT). This correspondence can be used as an argument for the unitarity of the evaporation of a black hole, since the dual CFT is a standard unitary gauge theory, albeit with a large number of color degrees of freedom N. The holographic dictionary states that the thermodynamics of AdS black holes is completely equivalent to the thermodynamics of the dual CFT. For instance, the entropy and temperature of a black hole match with the thermal entropy and temperature of the dual CFT, respectively. Moreover, the Hawking-Page first-order phase transition [4] between a large black hole and thermal AdS spacetime corresponds to the confinement/deconfinement phase transition of a quark gluon plasma [5].

In recent years, the thermodynamics of AdS black holes has been shown to feature a rich range of phenomena, including Van der Waals type phase transitions for charged AdS black holes [6–9], polymer transitions [10], reentrant phase transitions [11, 12], triple points [13, 14], superfluid transitions [15], and most recently multicriticality [16, 17]. These phenomena have been discovered in the context of extended phase space thermodynamics where the (negative) cosmological constant Λ is treated as a dynamical variable, and identified with a (positive) thermodynamic pressure according to [18–22]

$$P = -\frac{\Lambda}{8\pi G_N}\,, \qquad \Lambda = -\frac{(d-1)(d-2)}{2L^2}\,, \tag{1.1}$$

where L stands for the AdS curvature radius, G_N is the (fixed) Newton's constant, and d denotes the number of bulk spacetime dimensions. This identification gives rise to a new pair of conjugate variables in the first law of bulk thermodynamics — a pressure-volume term, $+V\delta P$, arises. The corresponding theory has come to be called *extended black hole thermodynamics*, or *black hole chemistry* (see [23] for a review). In particular, for a charged and multiply-spinning AdS black hole the first law and the generalised Smarr relation take the following form, respectively:

$$\delta M = T_H \delta S + \Phi \delta Q + \sum_i \Omega_i \delta J_i + V \delta P\,, \tag{1.2}$$

$$M = \frac{d-2}{d-3}\left(TS + \sum_i \Omega_i J_i\right) + \Phi Q - \frac{2}{d-3} PV\,. \tag{1.3}$$

Here, M stands for the mass of the black hole, T_H for the Hawking temperature, S for the Bekenstein-Hawking entropy, Q the electric charge and Φ the conjugate electrostatic potential. The angular momenta of the black hole are denoted by J_i, and their respective conjugate quantities are the relative angular velocities between horizon and infinity Ω_i [24], and V is the black hole thermodynamic volume — a quantity conjugate to the pressure P.

Very recently [25], a precise match has been found between the laws of extended black hole themodynamics and the laws governing the dual CFT. The key idea for this identification is to respect the conformal symmetry of the dual CFT, treating the AdS boundary conformal factor ω as a new thermodynamic parameter, so that the CFT volume $\mathcal{V}$ and the CFT central charge C can be varied independently, without needing to introduce a variable Newton's constant, as done in [26–31]. Namely, in this framework the conformal completion of the bulk AdS spacetime reads as

$$ds^2 = \omega^2\left(-dt^2 + L^2 d\Omega_{d-2}^2\right)\,, \tag{1.4}$$

where ω is an 'arbitrary' dimensionless conformal factor that is free to vary, reflecting the conformal symmetry of the boundary theory. Focusing on the spherical case, $d\Omega_{d-2}^2$ is the metric on a unit $(d-2)$-dimensional sphere, with the corresponding volume Ω_{d-2}. We take ω to be independent of the boundary coordinates, in which case the CFT volume reads

$$\mathcal{V} = \Omega_{d-2} R^{d-2}\,, \tag{1.5}$$

JHEP08(2023)142

where $R = \omega L$ is the variable curvature radius of the manifold where the CFT lives. The variation of the CFT volume $\mathcal{V}$ is then obviously independent of the variation of the central charge C, which for Einstein gravity is dual to

$$C = \frac{\Omega_{d-2} L^{d-2}}{16\pi G_N}\,, \tag{1.6}$$

even when Newton's constant G_N is held fixed. Employing the following AdS/CFT dictionary:

$$E = \frac{M}{\omega}\,, \quad T = \frac{T_H}{\omega}\,, \quad \tilde{\Omega} = \frac{\Omega}{\omega}\,, \quad \tilde{\Phi} = \frac{\Phi\sqrt{G_N}}{\omega L}\,, \quad \tilde{Q} = \frac{QL}{\sqrt{G_N}}\,, \tag{1.7}$$

it is easy to show that the bulk first law (1.2) is dual to [25, 27]:

$$E = T\delta S + \tilde{\Omega}\delta J + \tilde{\Phi}\delta\tilde{Q} + \mu\delta C - p\delta\mathcal{V}\,, \tag{1.8}$$

accompanied by the following two relations for the chemical potential μ associated to the central charge and for the pressure p, respectively,

$$\mu = \frac{1}{C}(E - TS - \tilde{\Omega}J - \tilde{\Phi}\tilde{Q})\,, \tag{1.9}$$

$$p = \frac{E}{(d-2)\mathcal{V}}\,, \tag{1.10}$$

known as the Euler relation and the equation of state for CFTs, respectively. This Euler equation holds for any large-N gauge theory, and differs from the standard one in thermodynamics in that it does not contain a $p\mathcal{V}$ term. In the high-temperature or large-volume regime, i.e. $RT \gg 1$, the μC term becomes equal to $-p\mathcal{V}$, and (1.9) becomes the standard thermodynamic Euler relation [27]. In ref. [32] we provided an extensive study of the extended thermodynamics of CFT states dual to charged, nonrotating AdS black holes.

It is the purpose of this paper to explore the implications of this proposal for rotating thermal CFT states that are dual to uncharged, singly-spinning AdS black holes in the bulk. In particular, we shall focus on the following three ensembles that feature interesting phase behavior:

$$\begin{aligned} &\text{fixed} \quad (J, \mathcal{V}, C): && F \equiv E - TS\,, \\ &\text{fixed} \quad (\tilde{\Omega}, \mathcal{V}, C): && W \equiv E - TS - \tilde{\Omega}J\,, \\ &\text{fixed} \quad (J, \mathcal{V}, \mu): && G \equiv E - TS - \mu C\,, \end{aligned} \tag{1.11}$$

where F, W, and G are the corresponding free energies of the respective ensembles. These ensembles are analogous to the three ensembles studied in [32] for thermal CFT states dual to charged, nonrotating AdS black holes, for which we found interesting phase behaviour. For the present rotating case, in the first ('canonical') ensemble, we shall show that there is a Van der Waals-like criticality for $d = 4, 5$, and reentrant phase transitions for $d \geq 6$. In the 'grand canonical ensemble', at fixed angular velocity and central charge, there is a first-order (de)confinement phase transition in all dimensions $d \geq 3$, following closely what happens in the bulk (see appendix A). Finally, the behavior of the free energy in the

JHEP08(2023)142

last ensemble, characterized by fixed angular momentum and chemical potential, is rather complex and unprecedented. It seems to indicate the presence of a plethora of zero-order phase transitions and unstable phases in both $d = 4$ and $d = 6$. However, one should be a bit cautious about the precise interpretation of these results, as this ensemble is novel and may come with presently unknown phases and instabilities that our analysis did not take into account.

Let us finally stress that the current analysis has a certain overlap with recent investigations [29, 30, 32–36]. In particular, the first two ensembles have been studied in $d = 4$ [33], in the context of the so-called *restricted phase space (RPS)* formalism. While similar in many technical aspects to our approach, the physical interpretation of RPS is very different from ours. Namely, in RPS the cosmological constant Λ is fixed in the bulk, while the gravitational constant G_N is varied.[1] Moreover, since on the CFT side in RPS one fixes $\omega = 1$, it implies that the CFT volume has to be held fixed and only the central charge remains a thermodynamic variable. Contrary to this, in our case, we hold Newton's constant fixed in the bulk and only vary Λ. However, by introducing general ω on the CFT side, both the CFT volume and the central charge are independently varied, subject to the two restrictions (1.9) and (1.10).

Our plan for the remainder of the paper is as follows. In section 2 we review singly-spinning AdS black holes in all dimensions and discuss their respective bulk and boundary thermodynamic quantities. Section 3 contains our main results regarding the phase behavior of the three thermodynamic ensembles. Section 4 is devoted to discussion of our results and conclusions. Appendix A reviews the grand canonical ensemble behavior of the singly-spinning black holes in the bulk, which is also compared to the (markedly different) fixed electrostatic potential ensemble for charged nonrotating AdS black holes. Additional technical details regarding the study of the $(J, \mathcal{V}, \mu)$ ensemble are gathered in appendix B.

2 Holographic thermodynamics of Kerr-AdS black holes

In this section we relate the extended thermodynamics of rotating black holes in AdS to the extended thermodynamics of the dual CFT. We keep the number of (bulk) spacetime dimensions d arbitrary in this section, while the detailed analysis of the CFT phase behavior in the next section will be carried out in $d = 4$ and $d = 6$, i.e. AdS_4/CFT_3 and AdS_6/CFT_5.

2.1 Extended bulk thermodynamics

We consider neutral singly-spinning black holes in asymptotically AdS spacetime, also known as Kerr-AdS black holes. These form a two parameter family of solutions to the vacuum Einstein equations with a negative cosmological constant, which were constructed

[1] Let us note here that a number of papers have considered the possibility of adding Newton's constant G_N to the *extended thermodynamic phase space*, e.g. [26–28, 37–39]. Since the inclusion of quantum corrections seems to indicate that G_N varies along the renormalization group flow, its variation in thermodynamics is perhaps plausible. However, such a treatment seems a bit problematic, in part since G_N is a constant of nature and varying G_N does not correspond to the original black hole chemistry. For this reason we try to avoid it in this paper.

JHEP08(2023)142

in four dimensions by Carter [40] and later generalized to higher dimensions in [41–43]. In Boyer-Lindquist coordinates, the Kerr-AdS line element in d spacetime dimensions reads

$$ds^2 = -\frac{\Delta}{\rho^2}(dt - \frac{a}{\Xi}\sin^2\theta d\phi)^2 + \frac{\rho^2}{\Delta}dr^2 + \frac{\rho^2}{\Sigma}d\theta^2 + \frac{\Sigma\sin^2\theta}{\rho^2}\left(adt - \frac{r^2+a^2}{\Xi}d\phi\right)^2 + r^2\cos^2\theta d\Omega_{d-4}^2\,, \tag{2.1}$$

where $d\Omega_{d-4}^2$ is the metric on the round unit $d-4$ sphere, and the various metric functions are given by

$$\Delta = (r^2+a^2)\left(1+\frac{r^2}{L^2}\right) - \frac{2m}{r^{d-5}}, \quad \Sigma = 1 - \frac{a^2}{L^2}\cos^2\theta, \quad \Xi = 1 - \frac{a^2}{L^2}, \quad \rho^2 = r^2 + a^2\cos^2\theta. \tag{2.2}$$

Here L is the AdS curvature radius given in (1.1), m is the mass parameter and a the rotation parameter. The mass parameter m can be expressed in terms of the other parameters and the outer horizon radius r_h (the largest positive real root of $\Delta = 0$) as

$$m = \frac{r_h^{d-5}}{2}(r_h^2 + a^2)\left(1 + \frac{r_h^2}{L^2}\right). \tag{2.3}$$

The expressions for the thermodynamic variables of the Kerr-AdS black hole in terms of the variables (r_h, a, L) are well known in the literature (see e.g. [42]). Here we provide a quick summary. The mass and angular momentum of Kerr-AdS black holes are given by

$$M = \frac{\Omega_{d-2}}{4\pi G_N}\frac{m}{\Xi^2}\left(1 + \frac{(d-4)\Xi}{2}\right), \qquad J = \frac{\Omega_{d-2}}{4\pi G_N}\frac{ma}{\Xi^2}. \tag{2.4}$$

The angular velocity of the black hole horizon relative to spatial infinity is

$$\Omega = \frac{a}{L^2}\frac{r_h^2 + L^2}{r_h^2 + a^2}. \tag{2.5}$$

The Hawking temperature is proportional to the surface gravity κ according to

$$T_H = \frac{\kappa}{2\pi} = \frac{1}{2\pi}\left[r_h\left(1+\frac{r_h^2}{L^2}\right)\left(\frac{1}{a^2+r_h^2} + \frac{d-3}{2r_h^2}\right) - \frac{1}{r_h}\right], \tag{2.6}$$

and

$$S = \frac{A}{4G_N} = \frac{\Omega_{d-2}}{4G}\frac{r_h^{d-4}(a^2+r_h^2)}{\Xi} \tag{2.7}$$

is the Bekenstein-Hawking entropy, proportional to the area A of the outer event horizon.

The thermodynamic volume can either be calculated from the extended first law (1.2), or from the Smarr relation (1.3). In either case we recover [19, 21]

$$V = \frac{r_h A}{d-1}\left[1 + \frac{a^2}{\Xi}\frac{1 + r_h^2/L^2}{(d-2)r_h^2}\right]. \tag{2.8}$$

Alternatively, this expression can also be computed by using a geometric approach. Indeed, it can be defined either in terms of surface integrals of the Killing potential [18] (see [21] for

JHEP08(2023)142

an explicit calculation using the proper gauge fixing of the Killing potential, as opposed to the background subtraction procedure proposed in [18]), or as the (background subtracted) Killing volume [44]

$$V = \int_{\Sigma_{\rm bh}} |\xi| dV - \int_{\Sigma_{\rm AdS}} |\xi| dV \,, \tag{2.9}$$

where $|\xi| = \sqrt{-\xi \cdot \xi}$ is the norm of the horizon generating Killing vector $\xi = \partial_t + \Omega \partial_\phi$. Let us now relate these bulk thermodynamic quantities to the boundary thermodynamic quantities of the dual CFT.

2.2 Extended boundary thermodynamics

In the AdS/CFT correspondence the dual CFT lives on the conformal boundary of the asymptotically AdS spacetime. According to [2, 3], the CFT metric is identified with the boundary metric of the dual asymptotically AdS spacetime up to a Weyl rescaling, $g_{\rm CFT} = \lim_{\rho\to\infty} \lambda^2(x) g_{\rm AdS}$, where ρ is a radial coordinate and $\lambda(x)$ is a Weyl scale factor. Following [24, 45], we take the boundary metric to be that of the Einstein static Universe (up to a constant Weyl factor ω), i.e. the standard product metric on $\mathbb{R} \times S^{d-2}$:

$$ds^2 = \omega^2 \Big(-dt^2 + L^2 d\Omega_{d-2}^2 \Big) \,. \tag{2.10}$$

To see how this arises from an asymptotic limit of the Kerr-AdS metric, we perform the following coordinate transformation [46]

$$\varphi = \phi - \frac{a}{L^2} t \,, \quad \rho \cos\Theta = r \cos\theta \,, \quad \rho^2 = \frac{1}{\Xi} (r^2 \Sigma + a^2 \sin^2\theta) \,, \tag{2.11}$$

where we focus for simplicity on $d = 4$ dimensions. This brings the $m = 0$ metric (2.1) to the following form:

$$ds^2 = -\Big(1 + \frac{\rho^2}{L^2}\Big) dt^2 + \frac{d\rho^2}{1 + \frac{\rho^2}{L^2}} + \rho^2 (d\Theta^2 + \sin^2\Theta d\varphi^2) \,. \tag{2.12}$$

By taking the limit $\rho \to \infty$ and multiplying with the Weyl factor $\lambda = \omega L/\rho$, we arrive at the CFT metric (2.10). Although the corresponding boundary metric is static, this is misleading as the regularity of the Euclidean section of the Kerr-AdS black hole requires the identification

$$(t, \rho, \Theta, \varphi) \sim (t + i\beta, \rho, \Theta, \varphi + i\beta\Omega) \,, \tag{2.13}$$

which gives rise to a rotating state on the boundary with linear velocity $v \equiv \Omega L$. Obviously, for

$$\Omega > 1/L \tag{2.14}$$

the Einstein Universe on the boundary rotates faster than the speed of light, and the corresponding CFT seems ill defined.[2] In the bulk, this corresponds to the classical *superradiant instability* of the corresponding small black hole solutions, which have horizon

[2] It was shown in [47], that a weakly coupled CFT does not admit a well-defined partition function when $\Omega L > 1$. While a good indication that 'something' may go wrong for $\Omega > 1/L$, our CFT is strongly coupled and the previous argument does not necessarily apply.

JHEP08(2023)142

radius $r_h < \sqrt{aL}$. As argued in [46], the endpoint of such an instability corresponds to a 'hairy black hole' with $\Omega L = 1$.

The existence of the bound (2.14) therefore imposes a restriction on the validity of the thermodynamic phase diagrams constructed below. One possibility is to disregard the superradiant/faster than speed of light branches from the free energy diagrams completely (see black curves therein). As such states often minimize the free energy, doing so would completely modify the thermodynamic behavior of the system and would imply novel phase diagrams (often characterized by additional zeroth-order phase transitions). However, physically it makes much more sense to assume that the superradiant/faster than speed of light branches will be replaced by the corresponding branches of stable 'hairy' black holes/novel phases of CFT that are in some sense thermodynamically "close to" the original $\Omega L > 1$ branches. For this reason in what follows we 'preserve' (apart from the grand canonical ensemble) the $\Omega L > 1$ branches in the free energy diagrams and construct the corresponding phase diagrams as if these branches remained present. We expect that this gives a qualitatively better picture than disregarding these branches completely.

The AdS formulae (2.4)–(2.7), together with the holographic dictionary (1.6) and (1.7), provide information about the (extended) thermodynamics of the dual large-N, strongly coupled CFT. In the next section, we will look at the implied thermodynamic phase behaviour of the CFT. For this purpose, it turns out to be convenient to introduce two dimensionless parameters,

$$x \equiv \frac{r_h}{L}\,, \qquad\qquad z \equiv \frac{a}{L}\,, \tag{2.15}$$

with which we have

$$\Sigma = 1 - z^2\cos^2\theta, \qquad \Xi = 1 - z^2, \qquad mL^{3-d} = \frac{x^{d-5}}{2}(x^2+z^2)\left(1+x^2\right)\,. \tag{2.16}$$

In terms of x and z, the CFT thermodynamic quantities are given by

- entropy:

$$S = 4\pi C x^{d-4}\frac{x^2+z^2}{1-z^2}\,, \tag{2.17}$$

- energy:

$$E = \frac{1}{R}4C\frac{x^{d-5}(x^2+z^2)\,(1+x^2)}{2(1-z^2)^2}\left(1+\frac{(d-4)(1-z^2)}{2}\right)\,, \tag{2.18}$$

- angular momentum:

$$J = 4C\frac{z}{(1-z^2)^2}\frac{x^{d-5}}{2}(x^2+z^2)\left(1+x^2\right)\,, \tag{2.19}$$

- temperature:

$$T = \frac{1}{2\pi R}\left[x\left(1+x^2\right)\left(\frac{1}{x^2+z^2}+\frac{d-3}{2x^2}\right)-\frac{1}{x}\right]\,, \tag{2.20}$$

- angular velocity:

$$\tilde{\Omega} = \frac{z}{R}\frac{x^2+1}{x^2+z^2}\,, \tag{2.21}$$

- chemical potential:

$$\mu = \frac{x^{d-5}\,(x^2-1)\,(x^2+z^2)}{R\,(z^2-1)}\,. \tag{2.22}$$

Note that the $1/R$ dependence in the formulas above is fixed by the scale invariance of the CFT, and the proportionality with C in equations (2.17)–(2.19) is due to the large-C limit of the CFT. In what follows we shall make use of these variables to analyze the different phases in the various thermodynamic ensembles in the dual CFT.

3 Thermodynamic ensembles in the dual CFT

In this section we study the phase behaviour of different "(grand) canonical" thermodynamic ensembles in the CFT, for thermal states that are dual to Kerr-AdS black holes. There are in principle eight grand canonical ensembles in the CFT, since at fixed temperature there are three pairs of conjugate thermodynamic variables, namely $(\tilde{\Omega}, J)$, $(p, \mathcal{V})$ and (μ, C). In this paper we concentrate on the following three ensembles that feature interesting phase behavior. We denote the associated free energies of the ensembles respectively as F, W and G:

$$\begin{aligned}
&\text{"canonical"} \quad (J, \mathcal{V}, C): && F \equiv E - TS = \tilde{\Omega} J + \mu C\,,\\
&\text{"grand canonical"} \quad (\tilde{\Omega}, \mathcal{V}, C): && W \equiv E - TS - \tilde{\Omega} J = \mu C\,,\\
&\text{"novel"} \quad (J, \mathcal{V}, \mu): && G \equiv E - TS - \mu C = \tilde{\Omega} J\,,
\end{aligned} \tag{3.1}$$

where, to obtain the second equalities, we have used the Euler equation (1.9). In each case we shall also study the associated heat capacity, which gives a measure of thermodynamic stability of the system. We shall denote these as

$$\mathcal{C}_\chi \equiv T \left(\frac{\partial S}{\partial T}\right)_\chi\,, \qquad \chi \in \{(J, \mathcal{V}, C), (\tilde{\Omega}, \mathcal{V}, C), (J, \mathcal{V}, \mu)\}\,. \tag{3.2}$$

Explicit expressions for the heat capacity in the latter two ensembles can be found below, while we omit the expression for $\mathcal{C}_\chi$ in the first ensemble because it is too lengthy. The characteristic features of $\mathcal{C}_\chi$ for the three ensembles are displayed below.

Before moving on, we would like to point out one recent related study in the literature. In [33], the authors studied the bulk thermodynamics of the rotating AdS black holes in $d = 4$ in the slowly rotating limit while keeping $\delta L = 0$ (referred to as "restricted phase space"). This is essentially equivalent to our fixed $\mathcal{V}$ ensembles (with $\omega = 1$). However, we are here interpreting the results from the point of view of the boundary CFT instead of the bulk gravity theory, and without going to the slowly rotating limit. The interested reader is thus invited to visit [33] to see how some of our results can be interpreted from the bulk perspective.

In what follows, the values for the dimensionful quantities $\{F, W, G, T, \tilde{\Omega}, \mu\}$ (including in all figures) will always be understood to be given in units $1/\ell$, where ℓ is an arbitrary constant length scale. Similarly, the values of $\mathcal{V}$ will be give in units of ℓ^{d-2}. Furthermore, we note from the expressions (2.17)–(2.22) that the scale R, and hence $\mathcal{V}$, does not affect the qualitative thermodynamic behaviour of the system. Hence we set $\mathcal{V} = 1$ in all illustrative figures.

JHEP08(2023)142

3.1 Canonical ensemble: $F(T, J, \mathcal{V}, C)$

The canonical (fixed T, J, P) ensemble has been well studied in the framework of black hole chemistry in the bulk [11, 48]. In those studies it was found that the smallest dimension that displays interesting phase behaviour is $d = 4$, where a *Van der Waals like phase transition* takes place between small and large rotating black holes. While the behaviour in $d = 5$ is qualitatively similar to $d = 4$, black holes in dimensions $d \geq 6$ can undergo *reentrant phase transitions*, which are absent in the lower dimensions. In this section we study the analogous ensemble in the CFT in $d = 4$ and $d = 6$, which is given by not only fixing the angular momentum, but also holding fixed the volume and central charge.

The relevant free energy in the fixed $(J, \mathcal{V}, C)$ canonical ensemble is

$$F = \frac{C x^{d-5}}{R\,(z^2-1)^2}\left(x^4\left(3z^2-1\right)+x^2\left(z^2+1\right)^2-z^4+3z^2\right). \tag{3.3}$$

We note that z in the above should be viewed as a function of C and J (and x), which can be obtained by inverting the expression (2.19) for J. While the actual solution is too long to be included here, we note from (2.19) that z is a function of x and of the ratio

$$\kappa \equiv J/C\,. \tag{3.4}$$

Together with the expressions (2.20) and (3.3) for T and F respectively, this implies that T and F/C are functions of $(x, \mathcal{V}, \kappa)$. We shall see the implications of this below.

3.1.1 $d = 4$: swallowtail criticality

Let us begin by considering the $F - T$ diagram in $d = 4$ dimensions (see figure 1). On the left, the value of J is kept fixed at $J = 1$, and the different curves correspond to varying $1/C$; the roles of J and $1/C$ are swapped on the right. These diagrams are reminiscent of the analogous diagrams for Van der Waals (VdW) fluids — the blue and yellow curves of these figures resemble the shape of a swallowtail. However these exist only *below* some *critical value*, $\kappa < \kappa_{4,\text{crit}}$, where we derive the numerical value for $\kappa_{4,\text{crit}}$ below in equation (3.10).

Each swallowtail consists of three piecewise smooth branches. Since the entropy (2.17) is an increasing function of x, we shall call the gently sloping branch starting from $T = 0$ the *low entropy (LE)* branch, as the value of x is the smallest on this branch. The steep, negatively sloped branch extending to $F \to -\infty$ is called the *high entropy (HE)* branch as x is largest on this branch. The intermediate branch joining these two has intermediate x values, and is called the *intermediate entropy (IE)* branch. For any swallowtail curve, starting at high T, the branch that minimizes the free energy and is thus thermodynamically favoured, is initially given by the HE branch. However at the self-intersection temperature, the $F-$minimizing branch changes to the LE branch. Standard thermodynamic arguments imply that the system, which in our case is a thermal CFT, undergoes a first-order phase transition at this temperature between the HE and LE phases. We note that these two phases have positive heat capacity $\mathcal{C}_{J,\mathcal{V},C}$ and hence are thermodynamically stable, while the IE branch has $\mathcal{C}_{J,\mathcal{V},C} < 0$, as can be seen in figure 5. This phase transition becomes second order at the *critical point* where the values of (J, C, T) are such that $J/C = \kappa_{4,\text{crit}}$

JHEP08(2023)142

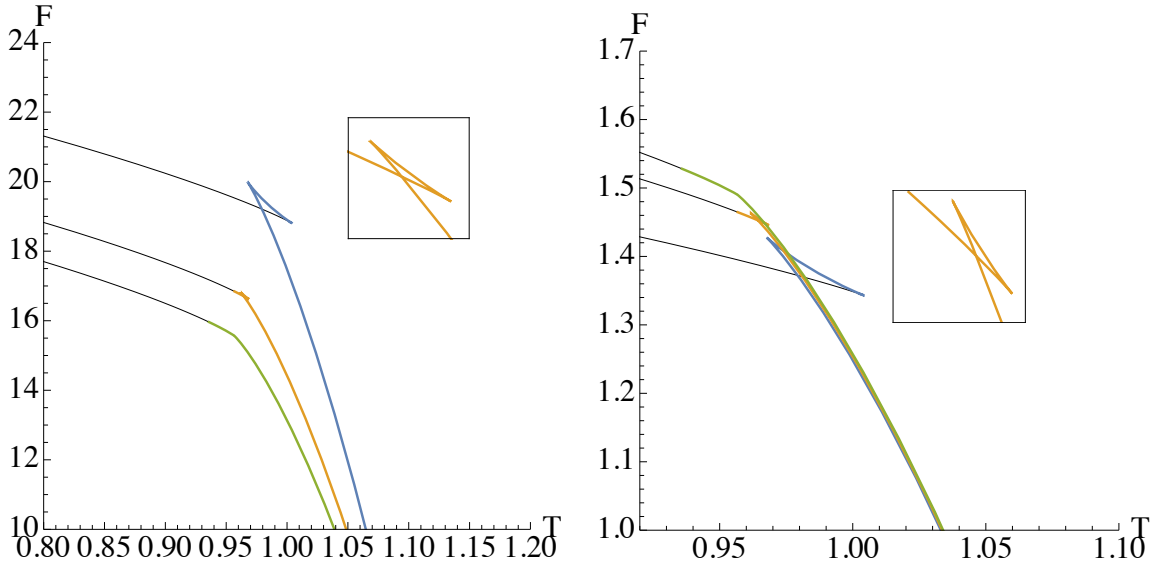

Figure 1. $F - T$ diagram of fixed $(J, \mathcal{V}, C)$ ensemble for $d = 4$, $\mathcal{V} = 1$. The free energy against temperature diagram is plotted here at $J = 1$ and various fixed C on the left, and $C = 1$ at various fixed J on the right. **Left**: $J = 1$, $C = 14$ (blue), $C = 11.5$ (yellow), $C \approx 10.45$ (green, critical). **Right**: $C = 1$, $J = 1/14$ (blue), $J = 2/23$ (yellow), $J \approx 0.0957$ (green, critical). The plot is swallowtail-shaped below a critical J/C ratio (see main text). Note that each curve in the left diagram is simply "stretched" along the F axis as compared to its counterpart on the right. The black portions of the curves denote the solutions with $\Omega L > 1$, where superradiant instabilities are present in the bulk. The insets show zoom-ins of the yellow swallowtail.

and $T = T_{\text{crit}}$. The $F - T$ curve (green) displays a kink at this critical point. Above the critical value for J/C the free energy curves will be smooth and single valued. This behaviour is typical swallowtail criticality, which is also present for charged AdS black holes [6].

A notable distinction from the standard first-order transitions seen for AdS black holes is that the smaller black hole branch has superradiant instabilities. In other words, as temperature decreases the first-order transition is from a large black hole to a small one with $\Omega L > 1$. This branch is presumably replaced with a branch of stable small black holes with some kind of scalar hair [46, 49]. We shall not pursue this issue further.

The co-existence phase diagrams for these transitions are plotted in figure 2. Each curve on these diagrams is a line of first-order phase transitions that terminates at a critical point denoted by open circles. The HE phase lies to the right of the curves while the LE phase lies to the left of the curves. The two phases become indistinguishable above the critical points. Notice that the left and right diagrams in figure 2 are identical. This is due to the above mentioned dependence of T and F/C on only the ratio J/C instead of on J and C independently. As a result, varying $1/C$ at fixed J has the same "thermodynamic effect" as varying J at fixed $1/C$. In particular, looking at figure 1, we see that each curve in the left diagram is only stretched along the F axis as compared to the corresponding curve on the right, but the phase transition temperatures are identical. This explains the identical diagrams in figure 2.

JHEP08(2023)142

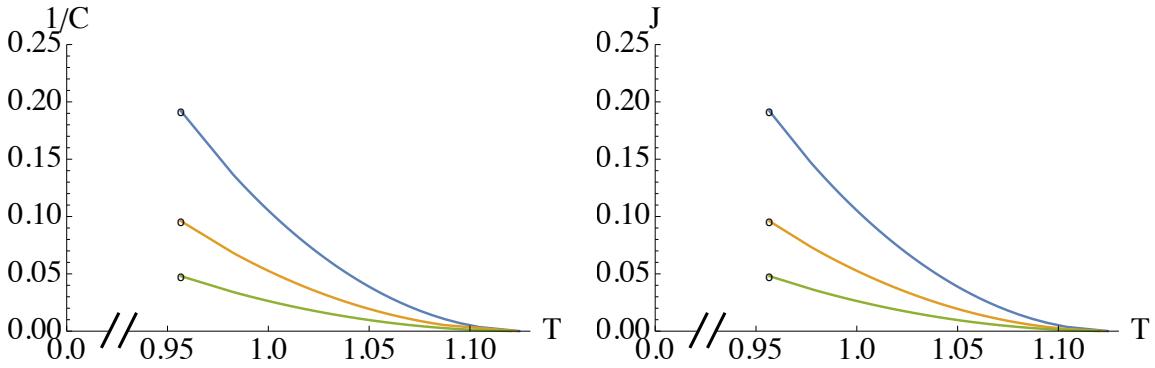

Figure 2. Co-existence diagram in $d = 4$. Each of the curves displayed here is a line of first-order phase transitions for different parameter values. **Left**: $J = 1/2$ (blue), $J = 1$ (yellow), $J = 2$ (green) for $\mathcal{V} = 1$. **Right**: $1/C = 1/2$ (blue), $1/C = 1$ (yellow), $1/C = 2$ (green) for $\mathcal{V} = 1$. For each of these parameter values, the line of first-order phase transition separates the low-entropy (LE) phase, lying to the left of the curve, and the high-entropy (HE) phase, lying to the right. Each line ends at a critical point, denoted by an open circle, where the phase transition becomes second order.

We also note that the T-intercepts of the co-existence lines all occur at the same value of T. This temperature is given by the Hawking-Page transition temperature T_{HP} at $J = 0$ which can be obtained by solving for x in (3.3) i.e., $F(x, z = 0) = 0$, for which one gets the solution $x = 1$ (or $r_h = L$). Substituting this and $z = 0$ into the expression for the temperature T then gives the value

$$T_{\text{HP}} = \frac{1}{\pi R}\,. \tag{3.5}$$

The thermodynamic behaviour in $d = 5$ is qualitatively similar to that in $d = 4$, displaying in particular the same swallowtail criticality. We shall not consider this case further.

3.1.2 $d = 6$: reentrant phase transition

The $F - T$ diagram for $d = 6$ is displayed in figure 3. For $\kappa < \kappa_{6,\text{crit}}$, each curve consists of four branches, allowing for more elaborate phase behaviour. In each case, one branch corresponds to a high-entropy state with positive heat capacity, and there is a low-entropy branch with negative heat capacity. The other two intermediate entropy branches have either negative or positive heat capacity, as can be seen on the right diagram of figure 5. Compared to the $d = 4$ case, the low-entropy branch with negative heat capacity is novel.

In the right diagram of figure 3, for sufficiently small J (the blue $J = 1/30$ curve) there is a cusp in the free energy diagram accompanied by an inverted swallowtail at higher temperatures, and so this case has only one phase. However for larger J the situation changes: the $J = 1/26$ (yellow) case implies a *reentrant phase transition*, where the inverted swallowtail now intersects the steep HE curve. Here the F-minimizing branch changes from the HE branch at (slightly) higher T to the LE branch before jumping back to the HE branch at some lower T. This last phase shall still be called the HE phase, though it has lower entropy than the original HE segment. This second transition is accompanied by

JHEP08(2023)142

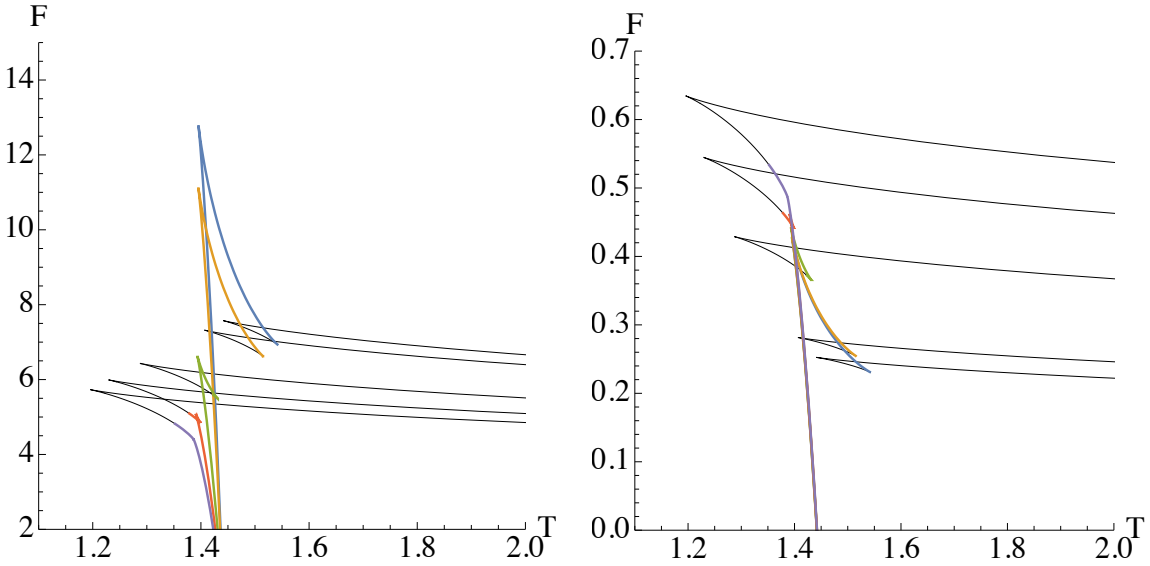

Figure 3. $F-T$ diagram of fixed $(J,\mathcal{V},C)$ ensemble for $d=6$, $\mathcal{V}=1$. **Left**: $J=1$, $C=30$ (blue), $C=26$ (yellow), $C=15$ (green), $C=11$ (red), $C\approx 9.03$ (purple, critical). **Right**: same values as left, with $J\leftrightarrow 1/C$. As in the $d=4$ case, the left diagram is simply a stretch of the right diagram along the F axis. The black portions of the curves denote the solutions with $\Omega L>1$, where superradiant instabilities are present in the bulk. Note that for the yellow and green curves there are HE to LE first-order transitions as the temperature decreases; however the LE branches are (partly) superradiant.

a jump in the free energy value and is hence a *zeroth-order phase transition* (ZOT). The line of ZOTs is depicted by the red line in the $J-T$ phase diagram of figure 4. As in the $d=4$ case, the $1/C-T$ phase diagram is qualitatively similar to figure 4 and is omitted.

For larger J (or smaller C) the situation changes further. The $J=1/15$ (green) case is an almost-star-shaped curve. As in the $d=4$ case, the steep negatively sloping branch has the largest x values. At high T, this HE branch initially minimises F but as T decreases there will be a first-order phase transition when this branch intersects the LE branch. These two branches have positive heat capacities, whereas the other two branches have negative heat capacities, as shown in figure 5.

For larger J we then have the familiar swallowtail corresponding to a first-order transition between the HE and LE states, up to the critical value (purple), with $J=0.11$. This behaviour is also visible in the phase diagram in figure 4, where we continue to see a line of first-order phase transitions, ending at a critical point depicted by an open circle. However, from the $F-T$ diagram, we see that the curves now do not intersect the $T=0$ axis unlike the $d=4$ case. This gives rise to an additional region in the phase diagram, lying to the left of the black line, where no solution exists. The black line intersects the $T-$axis at $T=\frac{\sqrt{15}}{2\pi R}$. This is the temperature at $J=0$ below which there is no solution (NS). From the $F-T$ diagram, we can observe that this happens at the minimum of $T(x)$, i.e. $\partial T/\partial x|_{z=0}=0$, which occurs at $x=\sqrt{d-3}/\sqrt{d-1}$. The same qualitative phase behaviour was found in $d=7$ and we did not find any new behaviours for higher dimensions.

JHEP08(2023)142

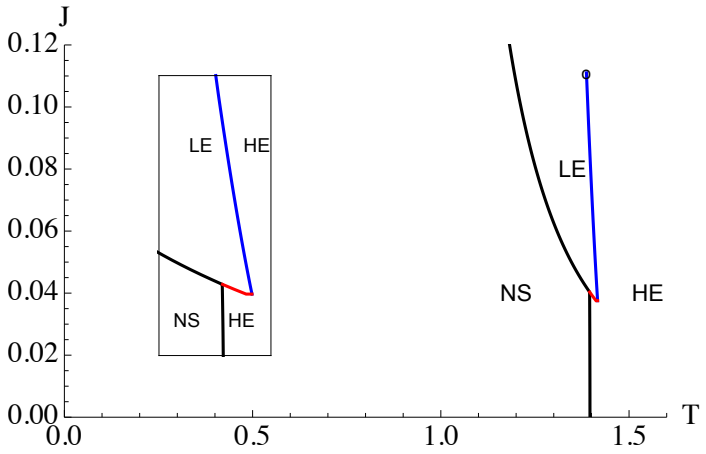

Figure 4. Phase diagram in fixed $(J, \mathcal{V}, C)$ ensemble, for $d = 6$ and $C = \mathcal{V} = 1$, showing a (blue) line of first-order phase transitions between high-entropy (HE) and low-entropy (LE) phases. The inset shows a close up around the (red) line of zeroth-order phase transitions between the LE and HE phases. The system can in fact undergo a HE-LE-HE reentrant phase transition as we lower J at a fixed temperature admitting zeroth-order phase transition. The region lying to the left of the black lines is a region where no solutions (NS) are possible.

3.1.3 Critical points

We now derive the numerical values of the critical point. In any d, the critical point is characterised by:

$$\frac{\partial C}{\partial \mu}\Big|_{T,J,\mathcal{V}} = 0 = \frac{\partial^2 C}{\partial \mu^2}\Big|_{T,J,\mathcal{V}} . \tag{3.6}$$

To this end, we first solve (2.20) for $z(T, R, x)$, and substitute this solution into (2.19) and (2.22) to obtain $C(J, x, z(T, R, x))$ and $\mu(R, x, z(T, R, x))$. This gives:

$$C = \frac{J x^{1-d} \left(-d x^2 - d + 4\pi R T x + x^2 + 5\right)^2 \sqrt{-\frac{x^2(d x^2+d-4\pi R T x - x^2 - 3)}{d x^2 + d - 4\pi R T x - 3x^2 - 5}}}{4\left(d x^2 + d - 4\pi R T x - x^2 - 3\right)} , \tag{3.7}$$

$$\mu = \frac{2\left(x^2 - 1\right) x^{d-3}}{(d-1)x^2 + d - 4\pi R T x - 5} . \tag{3.8}$$

From this we then solve numerically (3.6) for the critical point as the root of some polynomial equation whose degree depends on d. In $d = 4$ the critical point, which is C- and J-independent, is

$$T_{\rm crit} R \approx 0.26987 , \qquad x_{\rm crit} \approx 0.45882 , \tag{3.9}$$

corresponding to

$$\kappa_{4,\rm crit} \approx 0.095732 . \tag{3.10}$$

It is interesting to compare this to the result in [33], which found that $\kappa_{4,\rm crit} \approx 0.096424$ in the slowly rotating limit.

In $d = 6$ the critical point is,

$$T_c R \approx 0.612275 , \qquad x_c \approx 0.679425 , \tag{3.11}$$

JHEP08(2023)142

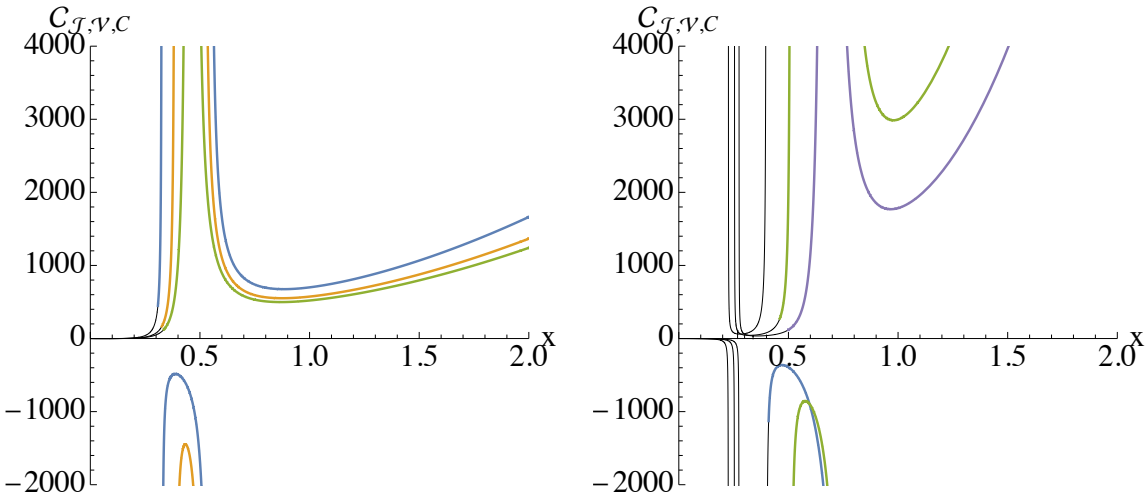

Figure 5. Heat Capacity $\mathcal{C}_{J,\mathcal{V},C}$ against x. The parameters used here are the same as those in figures 1 and 3, respectively. **Left:** $d = 4$, $J = 1$ and $C = 14$ (blue), $C = 11.5$ (yellow), $C \approx 10.45$ (green, critical). The first two curves obey $\kappa < \kappa_{4,\text{crit}}$ and consist of three piecewise continuous segments, corresponding to the three branches of the $F - T$ diagram: the LE, IE and HE phases. The LE phase corresponds to the segment with smallest x, having $\mathcal{C}_{J,\mathcal{V},C} > 0$; the IE phase has intermediate x and $\mathcal{C}_{J,\mathcal{V},C} < 0$; the HE phase has largest x and $\mathcal{C}_{J,\mathcal{V},C} > 0$. **Right:** $d = 6$, $J = 1$, $C = 30$ (blue), $C = 15$ (green), $C \approx 9.03$ (purple, critical). Here each curve with $\kappa < \kappa_{6,\text{crit}}$ consists of four piecewise continuous segments, in correspondence with the four branches in the $F - T$ diagram. Phase transitions take place between the two segments with $\mathcal{C}_{J,\mathcal{V},C} > 0$, corresponding to what was referred to as the LE (segment with relatively smaller x) and HE phases in the main text. Black lines correspond to superradiant phases in the bulk.

corresponding to

$$\kappa_{6,\text{crit}} \approx 0.1107\,. \tag{3.12}$$

3.2 Grand canonical ensemble: $W(T, \tilde{\Omega}, \mathcal{V}, C)$

Next we study the fixed $(\tilde{\Omega}, \mathcal{V}, C)$ ensemble, usually referred to as the "grand canonical ensemble". The free energy in this ensemble can be expressed as

$$W = \frac{C x^{d-5}\left(x^2-1\right)\left(x^2+z^2\right)}{R\left(z^2-1\right)} = \frac{C\left(\tilde{\Omega}R\left(z^2+1\right)-2z\right)\left(\frac{\sqrt{z-\tilde{\Omega}Rz^2}}{\sqrt{\tilde{\Omega}R-z}}\right)^{d-1}}{Rz(\tilde{\Omega}Rz-1)^2}\,, \tag{3.13}$$

where we have used

$$x = \frac{\sqrt{z-\tilde{\Omega}Rz^2}}{\sqrt{\tilde{\Omega}R-z}} \tag{3.14}$$

to obtain the second equality. Note that the condition $x > 0$ restricts the physical parameter values to $0 < z < \tilde{\Omega}R$, if $0 < \tilde{\Omega}R \leq 1$, and to $0 < z < 1/(\tilde{\Omega}R)$, if $\tilde{\Omega}R > 1$. In particular, as we shall see shortly, the point $(\tilde{\Omega}R, z) = (1, 1)$ corresponds to a 'transition point'.

JHEP08(2023)142

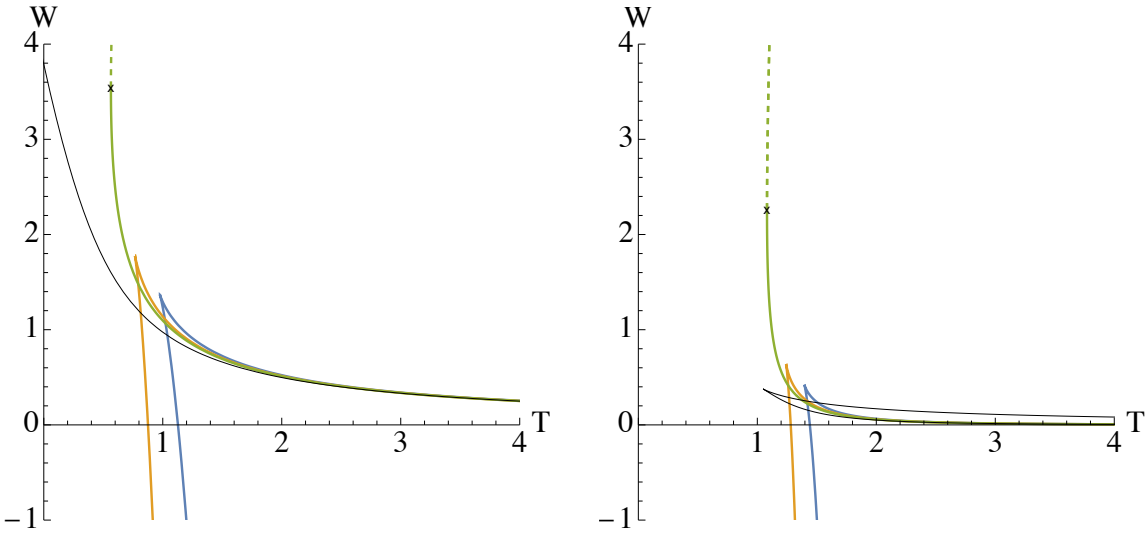

Figure 6. $W-T$ diagram of fixed $(\tilde{\Omega}, \mathcal{V}, C)$ ensemble for $\mathcal{V} = 1 = C$, $d = 4$ (left), and $d = 6$ (right). The curves correspond to $\tilde{\Omega}R = 1/20$ (blue), $\tilde{\Omega}R = 5/6$ (yellow), $\tilde{\Omega}R = 1$ (green) and $\tilde{\Omega}R = 3/2$ (black). For $\tilde{\Omega}R = 1$, the physical part of the figure corresponds to the solid line, while the dashed part has $z > 1$. The black lines correspond to superradiant black holes in the bulk.

Further, we can obtain the expression for the temperature in terms of the variables $(\tilde{\Omega}, R, z)$ in the same way, which yields

$$T = \frac{\tilde{\Omega}R\left(d-3-2\tilde{\Omega}Rz-(d-3)z^2\right)+2z}{4\pi R\sqrt{z(\tilde{\Omega}R-z)(1-\tilde{\Omega}Rz)}}\,. \tag{3.15}$$

This allows one to plot the $W-T$ diagram parametrically. We refer the reader to appendix A for the discussion of bulk thermodynamics in the grand canonical ensemble, for comparison.

3.2.1 (De)confinement phase transition

Let us first study the $W-T$ diagram, which is plotted in figure 6 for $d = 4$ (left) and $d = 6$ (right). For values of $\tilde{\Omega}R < 1$, the free energy vs. temperature diagram suggests that a first-order (Hawking-Page like) phase transition occurs at the point where the curve cuts the $T-$axis at

$$z = \frac{1-\sqrt{1-R^2\tilde{\Omega}^2}}{R\tilde{\Omega}}\,, \qquad T = \frac{d-3+\sqrt{1-R^2\tilde{\Omega}^2}}{2\pi R}\,. \tag{3.16}$$

This gives a line of first-order phase transitions on the $\tilde{\Omega}-T$ co-existence diagram, plotted in figure 7 for $\tilde{\Omega}R \geq 0$. For $\tilde{\Omega} = 0$ this agrees with the standard Hawking-Page phase transition at temperature $T_{\rm HP} = \frac{d-2}{2\pi R}$, but for nonzero angular velocity we have an entire line of phase transitions. We labeled the phase at low temperature as the *confined* phase, which is dual to thermal radiation in AdS, and the phase at higher temperature as the *deconfined* phase, which is dual to a large black hole. The deconfined phase dominates the ensemble if $W < 0$ solutions on any given $W-T$ curve for $\tilde{\Omega}R < 1$, while the confined

JHEP08(2023)142

phase dominates if the curve satisifes $W > 0$. The confined phase has $W = 0$, since we defined W in the bulk as the free energy of the black hole system minus that of thermal AdS.

Furthermore, for $\tilde{\Omega}R > 1$ the free energy W is greater than zero and the curves no longer intersect the $T-$axis. As a result, in this regime the $W-$minimizing phase is always given by the confined phase (see also [47]). When $\tilde{\Omega}R = 1$, the expressions for W and T reduce to

$$\tilde{\Omega}R = 1: \qquad W = \frac{z^{(d-3)/2}}{R}, \qquad T = \frac{(d-3)(z+1)}{4\pi R\sqrt{z}}. \tag{3.17}$$

In particular, if $z = 1$ we have $(T_\times, W_\times) := ((d-3)/(2\pi R), 1/R)$. This point is indicated by the cross ("x") in figure 6. The range $z > 1$ is plotted in figure 6 using dashed lines to indicate that this is an unphysical region with $a > L$, which corresponds to an overspinning black hole. This range is not included in the co-existence diagram in figure 7.

The behaviour here for the CFT dual to the Kerr-AdS family is markedly different from that dual to the analogous ensemble for the charged Reissner-Nordström AdS family. The latter has been studied for example in [32], with fixed electric potential $\tilde{\Phi}$, in place of the fixed angular velocity $\tilde{\Omega}$ here. Like in the rotating case, the free energy diagram displays a HP-like cusp for low $\tilde{\Phi}$ but becomes smooth for $\tilde{\Phi} > \Phi_c$ (see figure 16 in appendix A for the bulk version of the free energy diagram). However, while the deconfined phase here has $W > 0$ for $\tilde{\Omega}R \geq 1$, that of the charged case has $W \leq 0$ for $\tilde{\Phi} \geq \Phi_c$. This explains the difference between the co-existence diagrams in the rotating and charged case: in the former, the phase that dominates the grand canonical ensemble for $\tilde{\Omega}R \geq 1$ is the confined phase, while in the latter the phase that dominates for $\tilde{\Phi} \geq \Phi_c$ is the deconfined phase.

3.2.2 Heat capacity and thermal stability

We now examine the stability of the different phases as indicated by their heat capacity,

$$\mathcal{C}_{\tilde{\Omega},\mathcal{V},C} = -\left(\frac{\sqrt{z-\tilde{\Omega}Rz^2}}{\sqrt{\tilde{\Omega}R-z}}\right)^d \frac{4\pi C\left(\tilde{\Omega}R-z\right)}{z\left(\tilde{\Omega}Rz-1\right)^2} \times \tag{3.18}$$
$$\times \frac{\left(-\left((d-4)z^2\right)+2(d-3)\tilde{\Omega}Rz-d+2\right)\left((d-3)\tilde{\Omega}R\left(z^2-1\right)+2\tilde{\Omega}^2R^2z-2z\right)}{(d-3)\tilde{\Omega}R\left(z^4+6z^2+1\right)-2\tilde{\Omega}^2R^2z\left((d-2)z^2+d-4\right)-2z\left((d-4)z^2+d-2\right)}.$$

We plot the heat capacity $\mathcal{C}_{\tilde{\Omega},\mathcal{V},C}$ against the temperature T in figure 8. From this we see that for $\tilde{\Omega}R < 1$ the lower branch of the $W - T$ diagram has positive heat capacity and is therefore thermodynamically stable, while the upper branch has negative heat capacity. Moreover, the heat capacity is negative in $d = 4$ for $\tilde{\Omega}R \geq 1$, and in $d = 6$ it is negative for $\tilde{\Omega}R = 1$. Further, the heat capacity of the solution with $\tilde{\Omega}R \geq 1$ in $d = 6$ has an interesting feature: the upper branch in the $W - T$ diagram (black curve in figure 6) has negative heat capacity, while the lower branch has negative heat capacity for large temperatures but positive heat capacity for small temperatures. The positive heat capacity for small temperatures is a novel feature in six dimensions compared to four dimensions.

JHEP08(2023)142

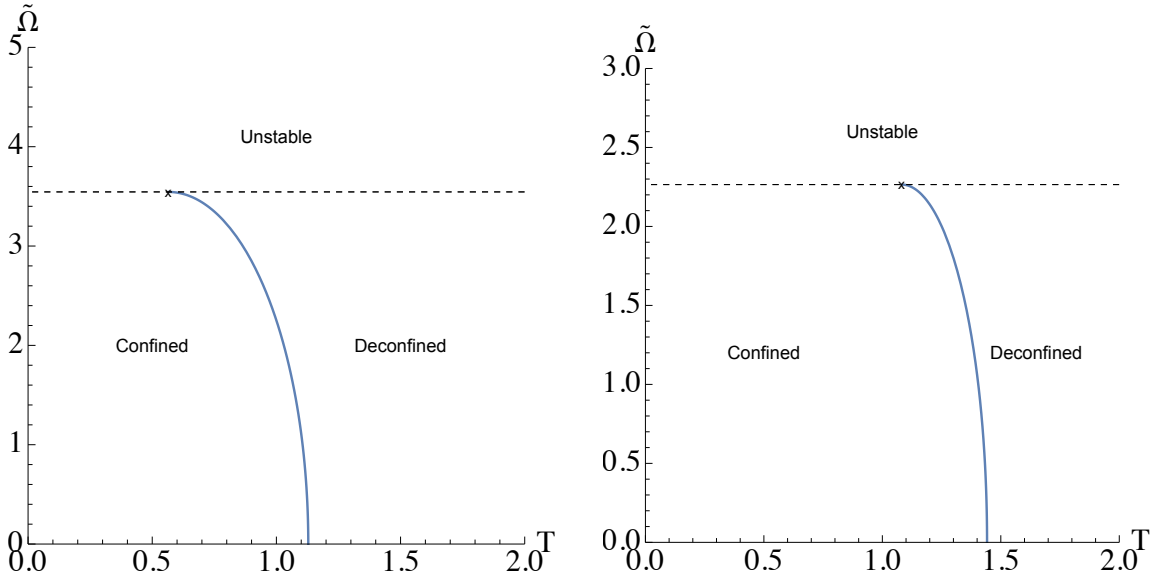

Figure 7. Co-existence diagram for $\tilde{\Omega}$ vs. T. The parameters used here are $C = 1 = \mathcal{V}$, $d = 4$ (left), and $d = 6$ (right). For $\tilde{\Omega}R < 1$, a first-order phase transition occurs across the co-existence line separating the confined and deconfined phase. Contrary to the canonical ensemble, the coexistence line no longer terminates at a critical point. Rather, an 'unstable region' (subject to superradiant instabilities in the bulk) develops for $\tilde{\Omega}R \geq 1$.

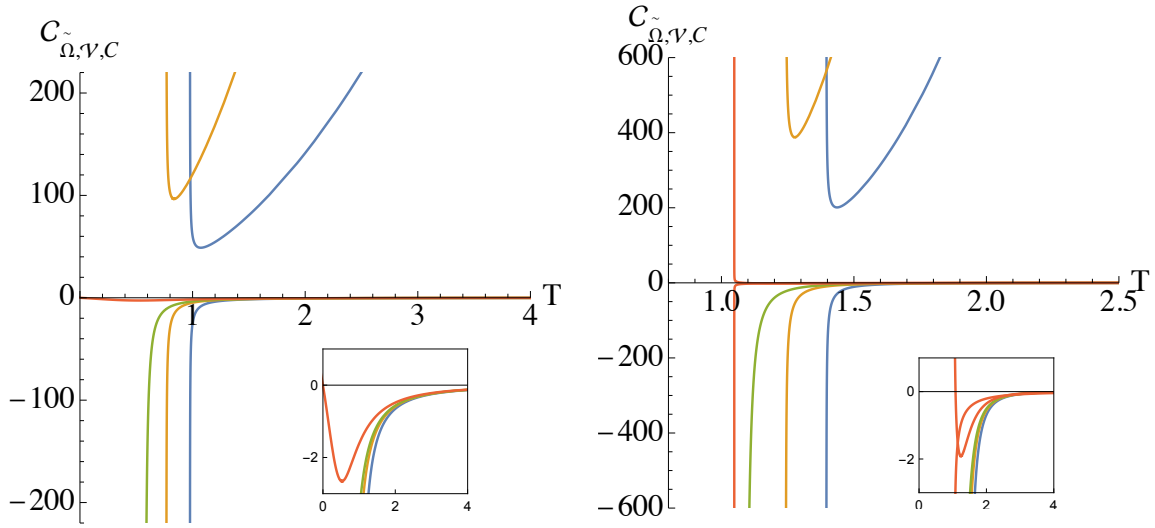

Figure 8. Heat capacity $\mathcal{C}_{\tilde{\Omega},\mathcal{V},C}$ against temperature T for $\mathcal{V} = 1 = C$, $d = 4$ (left), and $d = 6$ (right). The curves correspond to $\tilde{\Omega}R = 1/20$ (blue), $\tilde{\Omega}R = 5/6$ (yellow), $\tilde{\Omega}R = 1$ (green) and $\tilde{\Omega}R = 3/2$ (red), the same values as in figure 6. For each $\tilde{\Omega}$, the position of the vertical asymptote (if one exists) happens at the value of T at which the $W - T$ diagram experiences a cusp. For $\tilde{\Omega}R < 1$, the heat capacity has two branches: the positive branch corresponds to the lower branch in figure 6, while the negative $\mathcal{C}_{\tilde{\Omega},\mathcal{V},C}$ branch corresponds to the upper branch. For $\tilde{\Omega}R = 1$, $\mathcal{C}_{\tilde{\Omega},\mathcal{V},C} < 0$. For $\tilde{\Omega}R > 1$, $\mathcal{C}_{\tilde{\Omega},\mathcal{V},C} < 0$ in $d = 4$, while it has two branches in $d = 6$ (see insets for zoom-in around origin). The (red) branch with a minimum point corresponds to the lower (black) branch in figure 6.

JHEP08(2023)142

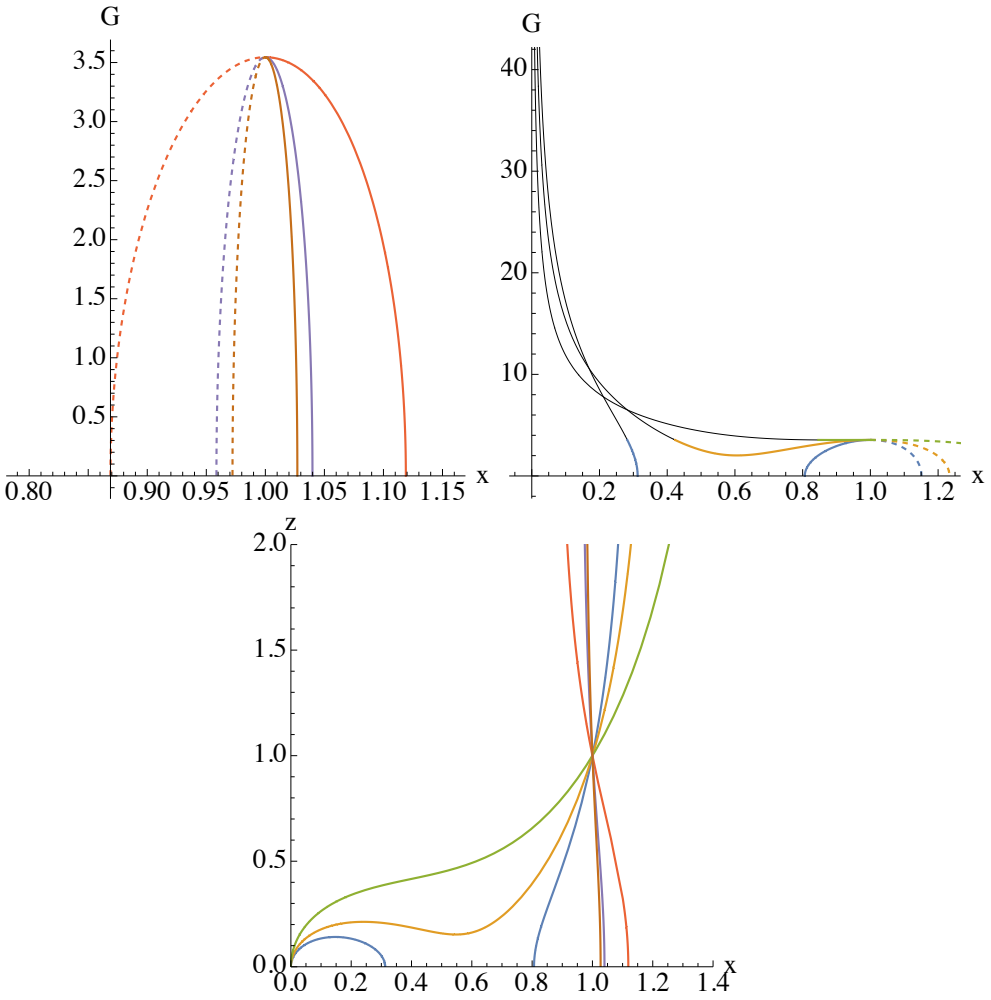

Figure 9. Physical ranges of x. The parameters used for the plots here are $d = 4$, $\mathcal{V} = 1$, $J = 1$, $\mu = -1$ (red), $\mu = -0.3$ (purple), $\mu = -0.2$ (brown), $\mu = 1$ (blue), $\mu = 3/2$ (yellow), $\mu = 3$ (green). The physical range of x is limited to those values for which $z \leq 1$. From the bottom figure, observe that for $\mu > 0$, this corresponds to $x < 1$ while for $\mu < 0$, this corresponds to $x > 1$. The physical ranges are depicted using solid lines in the $G - x$ plots, while the $z > 1$ regions are dashed. The same applies to the other plots in this section. The black lines correspond to superradiant states.

3.3 Novel ensemble: $G(T, J, \mathcal{V}, \mu)$

Finally, we study the ensemble in which the chemical potential μ for the central charge is kept fixed, while the central charge itself is allowed to vary. Although the physical meaning of this ensemble is not entirely clear, fixing μ corresponds to fixing W/C, or in other words fixing the thermal free energy per degree of freedom.

The free energy G and temperature T in the fixed $(J, \mathcal{V}, \mu)$ ensemble can be expressed as

$$G = \frac{2Cx^{d-5}z^2\left(x^2+1\right)^2}{R\left(z^2-1\right)^2} = J\frac{z}{R}\frac{x^2+1}{x^2+z^2} = \frac{J}{R}\sqrt{\left(1+\frac{1-x^2}{\mu R x^{5-d}}\right)\left(1+\frac{x^4-x^2}{\mu R x^{5-d}}\right)}, \quad (3.19)$$

JHEP08(2023)142

and

$$T = \frac{1}{4\pi\mu R^2}\left[\mu R\left((d-1)x + \frac{d-5}{x}\right) - 2x^{d-4}\left(x^2-1\right)\right], \tag{3.20}$$

by using the following expression for the rotation parameter z:

$$z = \sqrt{\frac{x^4 - x^2 + \mu R x^{5-d}}{1 - x^2 + \mu R x^{5-d}}}\,. \tag{3.21}$$

The above expressions for $G(x, J, \mathcal{V}, \mu)$ and $T(x, \mathcal{V}, \mu)$ allow us to parameterically plot the $G-T$ diagram using x as the parameter. However, the physical range of x is limited to values for which $z(x) < 1$, since from eqs. (2.15) $z > 1$ corresponds to an overspinning black hole with $a > L$, while eq. (2.17) shows that $S < 0$ when $z > 1$. Using (3.21) we plot $z(x)$ in the bottom diagram of figure 9 for $d = 4$ as an illustration. From this and (3.21), we see that the physical ranges of x are $x < 1$ for $\mu > 0$ and $x > 1$ for $\mu < 0$. Nonetheless, we continue to plot the unphysical ranges in the following $G-T$ figures, but denoting the $S < 0$ region with *dashed lines*. As in the previous two ensembles, we shall study the $G-T$ behaviour in $d = 4$ and $d = 6$.

3.3.1 $d = 4$: zeroth-order phase transitions

The first feature of this ensemble is the different behaviour exhibited by the system when $\mu < 0$ and $\mu > 0$. For example in $d = 4$, the $G-T$ diagram shows a single "dome" (see figure 10, top left) for $\mu < 0$, while for small $\mu > 0$, the dome is accompanied by a bigger quarter-arc (e.g. blue curve in figure 10, top right). In both cases, the $G-T$ graphs for different μ all intersect at the dashed-solid boundary point, $(T_i, G_i) = ((d-3)/(2\pi R), J/R)$, corresponding to $x = 1$.

Hence, the system has only a single phase when $\mu < 0$ but we can identify multiple phases for $\mu > 0$. As in the above ensembles, we label these phases according to their relative x values. For $\mu = 1$ (blue) in figure 10, x is smaller on the upper quarter-arc (cf. figure 9, bottom), which we label the low-entropy (LE) phase, whereas the high-entrop (HE) phase refers to the inner dome. As μ gets larger, the domes move closer together, eventually joining at a cusp for sufficiently large μ. For larger μ the cusp moves upward and leftward, as shown by the yellow curve.

The second feature to note in this ensemble is that all phase transitions are accompanied with a jump in G; in other words, they are *zeroth-order phase transitions*. As usual, for any fixed μ if the $G-T$ diagram is multi-branched (considering only the solid $z > 1$ regions), the branch with the lowest free energy G is thermodynamically favoured. A phase transition between different branches is implied whenever the $G-$minimizing branch changes. The bottom diagram of figure 10 shows all the implied phase transitions on the $\mu - T$ phase diagram. For example at $\mu = 1$, corresponding to the blue curve at the top right, there is no solution (NS) at high temperature. As T decreases, the LE solution is admitted; the system crosses the NS/LE boundary on the $\mu - T$ diagram. As T decreases further, the HE phase emerges with a lower value of G, giving rise to a LE/HE zeroth-order phase transition. The HE phase terminates at the $z = x = 1$ boundary (the solid-dashed boundary point of the $G-T$ curve) and the system undergoes another zeroth-order phase

JHEP08(2023)142

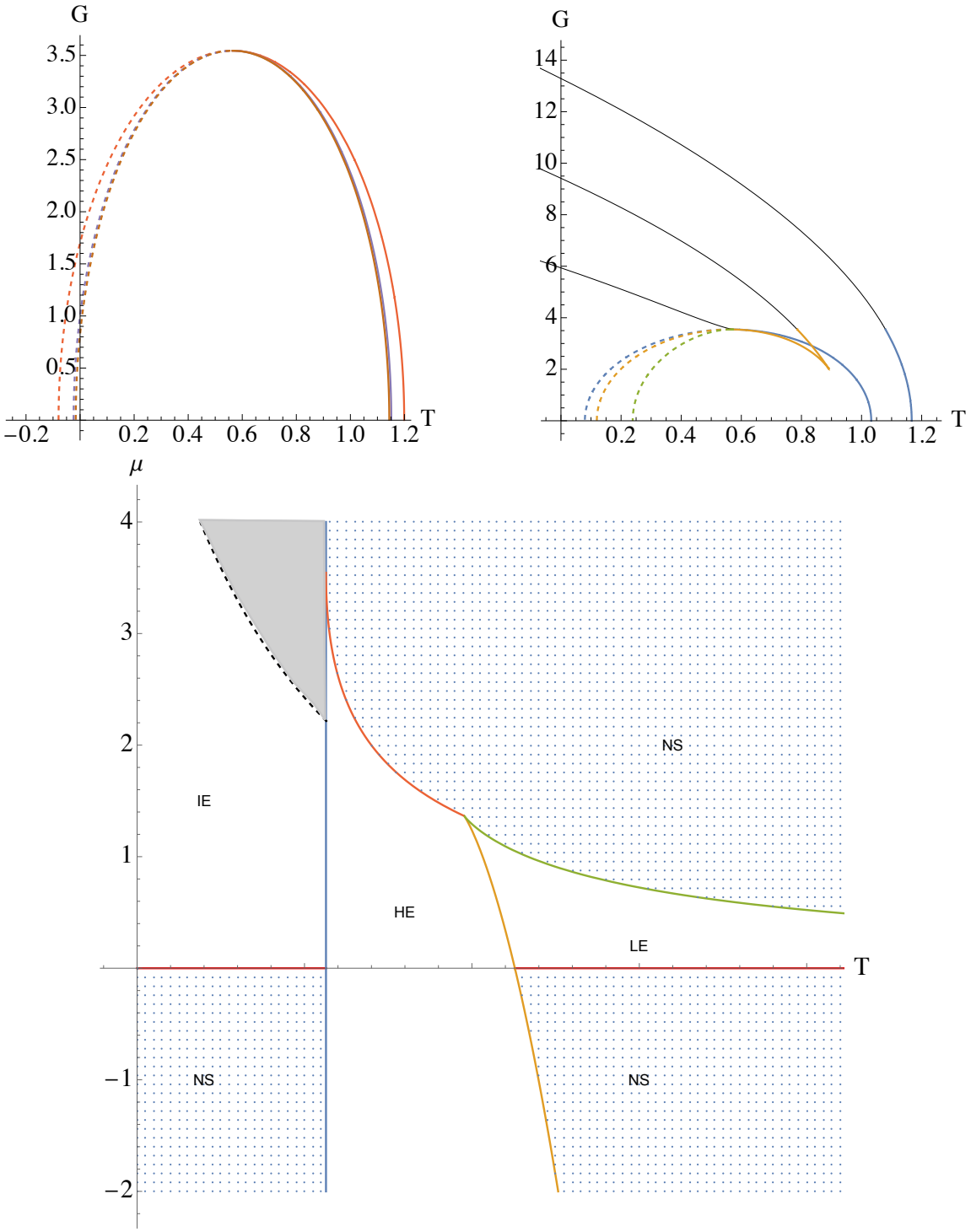

Figure 10. Thermodynamic behaviour in fixed $(\mathcal{J}, \mathcal{V}, \mu)$ ensemble for $d = 4$. The figures here are plotted for $\mathcal{V} = 1$, $J = 1$. **Top left:** $G - T$ free energy diagram for $\mu < 0$, $\mu = -1$ (red), $\mu = -0.3$ (purple), $\mu = -0.2$ (brown). **Top right:** $\mu > 0$, $\mu = 1$ (blue), $\mu = 3/2$ (yellow), $\mu = 3$ (green); the black portions of the curves denote the solutions with $\tilde{\Omega} R > 1$, where superradiant instabilities are present in the bulk. **Bottom:** co-existence phase diagram. Across each solid curve a zeroth-order phase transition takes place between the indicated phases. The IE phase is further split into a region with positive heat capacity $\mathcal{C}_{\mathcal{J},\mathcal{V},\mu}$ and a region with negative heat capacity (shaded).

JHEP08(2023)142

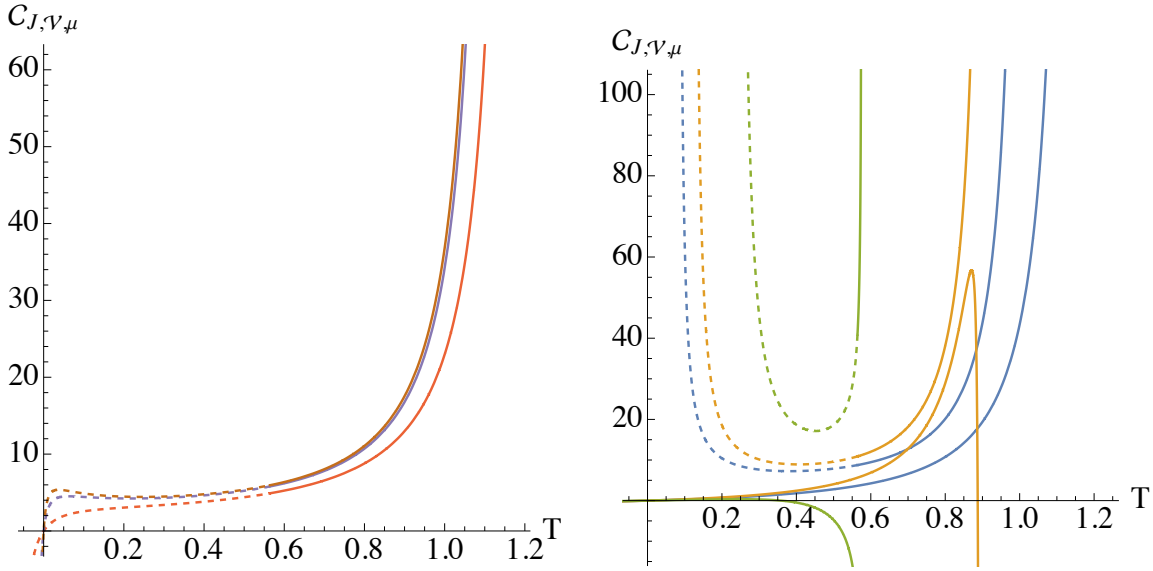

Figure 11. Heat capacities in fixed $(J, \mathcal{V}, \mu)$ ensemble for $d = 4$. **Left:** $\mu < 0$, $\mu = -1$ (red), $\mu = -0.3$ (purple), $\mu = -0.2$ (brown); **Right:** $\mu > 0$, $\mu = 1$ (blue), $\mu = 3/2$ (yellow), $\mu = 3$ (green).

transition to the intermediate entropy (IE) phase. The IE phase is further divided into a stable region with positive heat capacity $\mathcal{C}_{\mathcal{J},\mathcal{V},\mu}$, and an unstable region (shaded) with negative heat capacity. The other phases in the $\mu - T$ plot are all stable (cf. figure 11).

The explicit expression for the heat capacity in $d = 4$ is

$$\mathcal{C}^{d=4}_{\mathcal{J},\mathcal{V},\mu} = \frac{\pi \mathcal{J} \mu R \sqrt{x} \left(4\mu R x^3 + (x^2-1)^3\right) \left(x\left(3\mu R x - 2x^2 + 2\right) - \mu R\right)}{(-\mu R - x^3 + x)^{3/2} \left(-\mu R x + x^2 - 1\right)^{3/2} \left(\mu R + 3\mu R x^2 - 4x^3\right)}, \tag{3.22}$$

which we plot in figure 11.

3.3.2 $d = 6$: unstable small entropy phase

A similar analysis can be done for $d = 6$. The $G-T$ and corresponding $C_{J,\mathcal{V},\mu}-T$ diagrams for $\mu > 0$ and $\mu < 0$ are shown in figures 12 and 13, respectively, where

$$\mathcal{C}^{d=6}_{\mathcal{J},\mathcal{V},\mu} = \frac{\pi \mathcal{J} \mu R x^2 \left(\mu R + 5\mu R x^2 - 2x^5 + 2x^3\right) \left(4\mu R\left(2x^2-1\right) + 3x\left(x^2-1\right)^3\right)}{(-\mu R + x^3 - x)^{3/2} \left(-\mu R - x^5 + x^3\right)^{3/2} \left(-\mu R + 5\mu R x^2 - 8x^5 + 4x^3\right)} \tag{3.23}$$

is the explicit expression for the heat capacity in $d = 6$. While these look more complicated than in $d = 4$, the main information is contained in the $\mu - T$ phase diagram, figure 14. Similar to figure 10, obtaining this figure is straightforward but tedious. We leave the details to appendix B and comment here only on the main features. In this diagram, a zeroth-order phase transition again takes place across each solid curve (except of course at the NS boundary). In fact, the structure of this diagram is somewhat similar to the $d = 4$ case. However, unlike $d = 4$, for $\mu > 0$ solutions now extend to large T thus replacing the NS region in the upper right portion of the diagram in $d = 4$ by an LE phase in $d = 6$. This

JHEP08(2023)142

phase has negative heat capacity and so is unstable, as is evident from the lower diagrams in figure 12. Another distinction between the two cases is that the NS boundary in $d = 4$ which lies on (part of) the $T-$axis is now given by two curves in the $\mu > 0$ region, both terminating at a finite value of μ.

Finally, we note from (3.20) that T does not depend on J, while G only depends on J through an overall factor in all d (see eq. (3.19)). As a result, changing the value of J has a trivial effect on the figures presented in this subsection: for the $G - T$ figures, changing J only stretches the curves along the $G-$axis while all zeroth-order phase transitions occur at the original T values. Consequently the $\mu - T$ phase diagrams are independent of J, unlike in the fixed $(J, \mathcal{V}, C)$ ensemble.

4 Discussion

We have studied the thermodynamic phase transitions of thermal CFT states dual to Kerr-AdS black holes. The inclusion of the conjugate thermodynamic pair (C, μ) (the central charge and its associated chemical potential) increases the number of possible thermodynamic ensembles to eight — we have uncovered interesting phase behavior in three of them.

In previous studies, it was argued that the (inverse) central charge plays a similar role to the thermodynamic pressure $P \propto 1/L^2$ in the bulk thermodynamics of AdS black holes [11, 48, 50]. However as explained in [25, 27, 32] and in the introduction, this does not lead to a satisfactory duality between the bulk and boundary thermodynamics. To achieve this latter goal, one needs to either view Newton's constant G_N as a variable whose variation is related to variations in the CFT central charge, or introduce a new scale R for the radius of the CFT sphere. We find the latter scenario much more plausible. In addition, a reshuffling and rescaling of thermodynamic variables is needed to arrive at the holographic dictionary (1.7) which gives a clean duality between bulk and boundary first laws and Smarr relations.

In this new setting, we find that all the interesting phase behaviours in [6, 11, 48, 50] are preserved by the CFT — this is unsurprising, since we are simply replacing $P \propto 1/L^2$ by the new thermodynamic variable $C \propto L^{d-2}$. In particular, there continues to be swallowtail criticality in the fixed $(J, \mathcal{V}, C)$ ensemble for $d = 4$, as well as reentrant phase transitions for $d = 6$. However, we also note some new features. The $1/C - T$ coexistence curve is negatively sloped and cuts the $T-$axis in $d = 4$ at the Hawking-Page temperature $T_{\rm HP} = 1/\pi R$. Furthermore, the critical temperature is independent of C and J, unlike in [11, 48, 50], where the critical temperature was found to be $\propto 1/\sqrt{J}$. This difference can also be easily understood as follows: our CFT temperature has been rescaled as compared to the bulk Hawking temperature T_H in eq. (1.7), specifically, we have $T \propto T_H/\sqrt{P}$. At the critical point, the old bulk pressure behaves as $P_{\rm crit} \propto 1/J$, thus cancelling the $1/\sqrt{J}$ dependence of the critical temperature.

We emphasise that the role of the central charge C here is unconventional insofar as studies of phase transitions of a given system generally relate to the near equilibrium dynamics of a fixed theory; changing the central charge C relates instead to variations

JHEP08(2023)142

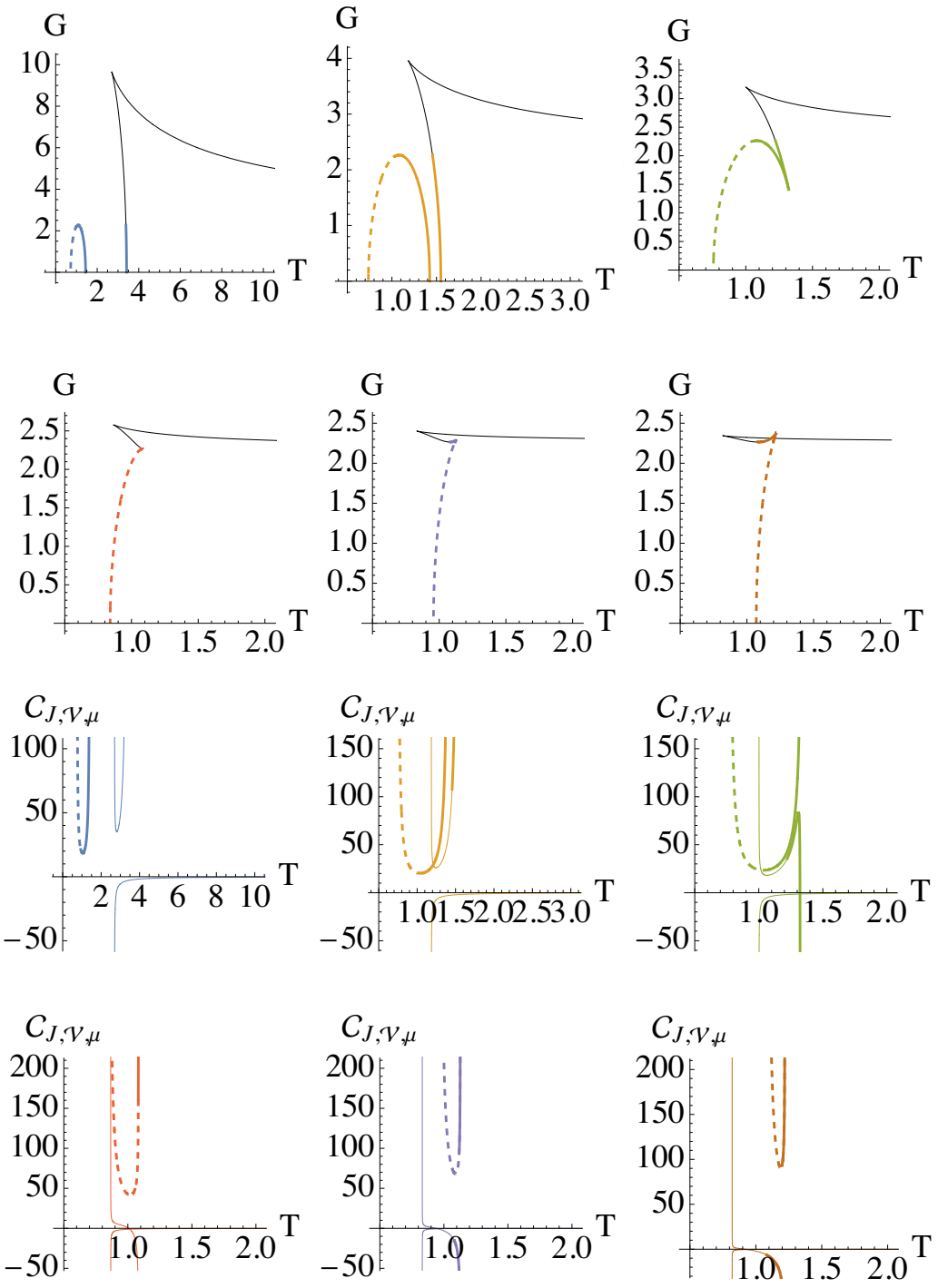

Figure 12. $G-T$ diagrams and heat capacities for $\mu > 0$ in $d = 6$. These are plotted for different illustrative μ values. Specifically, the parameters used here are $\mathcal{V} = J = 1$, and for the $G-T$ digrams on the first two rows, starting from the top left, we plotted $\mu = 0.01, 0.2, 0.5, 2, 5, 9$. The black portions of the curves denote the solutions with $\tilde{\Omega}R > 1$. The same parameters are used for the analogous heat capacity plots in the last two rows.

JHEP08(2023)142

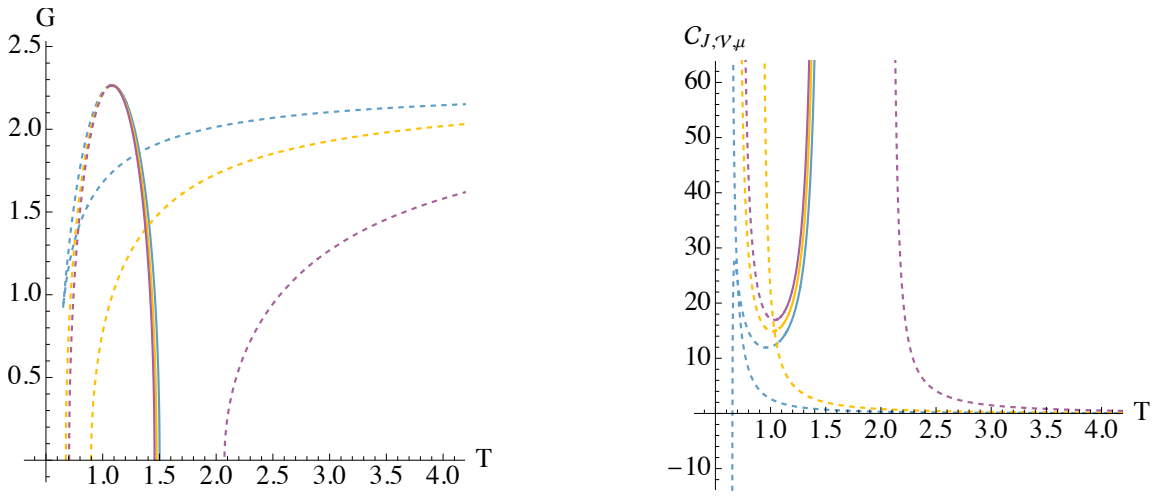

Figure 13. $G-T$ diagram and heat capacities for fixed $(J,\mathcal{V},\mu)$ ensemble with $\mu<0$ in $d=6$. The parameters used here are $\mathcal{V}=J=1$, $\mu=-1$ (blue), $\mu=-0.5$ (yellow), $\mu=-0.2$ (purple).

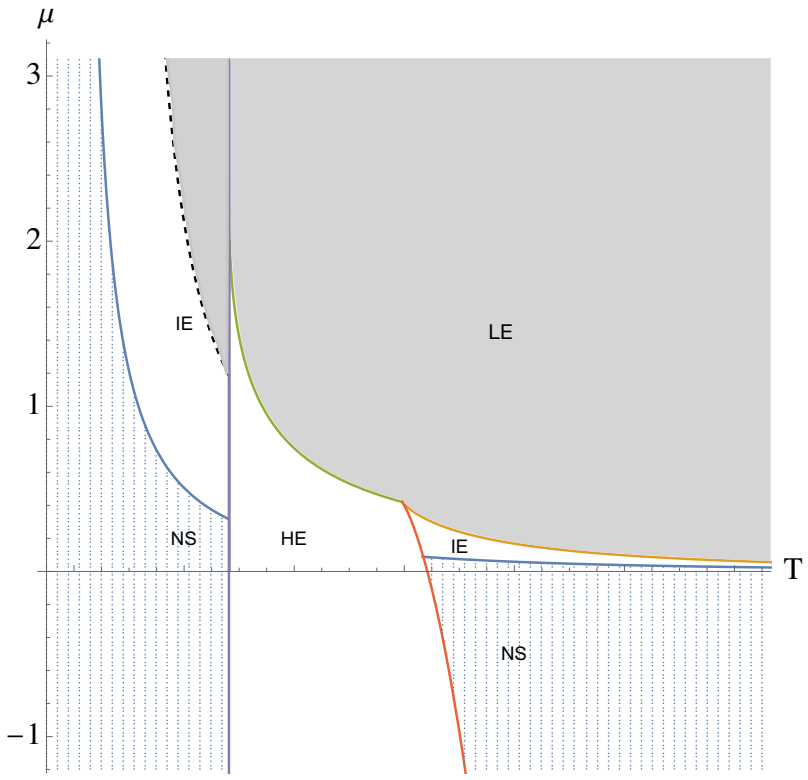

Figure 14. $\mu-T$ phase diagram in $d=6$, which follows from analysing the $G-T$ free energy diagrams in figure 12 and 13. Across each curve a zeroth-order phase transition (finite jump in G) takes place between the labeled phases. There are also regions (NS) where no solution exists at the given $(\mu,T,\mathcal{V}=1)$. The left IE phase is further split into a region with positive heat capacity $\mathcal{C}_{\mathcal{J},\mathcal{V},\mu}$ and a region with negative heat capacity (shaded).

JHEP08(2023)142

within an ensemble of theories.[3] We note that this is not without precedent. For example in [53], the authors considered a family of two-dimensional CFTs by taking symmetric products and studied the grand canonical ensemble by introducing a chemical potential conjugate to the number of copies of CFTs (the central charge of the symmetric product CFTs is proportional to this number). In the current context, the observed swallowtail criticality is interesting in its own right — it implies that within the current ensemble of rotating CFT theories, only those with a sufficiently large C can undergo a first-order Van de Waals' like phase transition.

Next, in the fixed $(\tilde{\Omega}, \mathcal{V}, C)$ ensemble we find a (de)confinement phase transition for $\tilde{\Omega}R < 1$. This is dual to the black hole/radiation Hawking-Page like phase transition of the Kerr-AdS black hole. Furthermore, in the peculiar fixed $(J, \mathcal{V}, \mu)$ ensemble, we observe several novel zeroth-order phase transitions between the various CFT phases (see figures 10 and 14). Moreover, at certain parameter ranges, the phase diagram suggests a transition from a phase with positive heat capacity to one with negative heat capacity. A similar transition was also observed in CFTs dual to charged AdS black holes in the fixed chemical potential ensemble [32]. We caution that while these are interesting new features, the physical viability of zeroth-order phase transitions in nature is unknown. In addition, a physical interpretation of the fixed μ ensembles is elusive — it is unclear how one can prepare a system with fixed μ while allowing the central charge to vary.

We have also noted the presence in all ensembles of classical superradiant instabilities in the bulk, previously observed in [50]. It is an interesting question as to what this classical instability means for the CFT or even the bulk black hole as a thermodynamic system. Classically, a small perturbation to a superradiant black hole will lead to a decay to another non-superradiant black hole with slower rotation; hence one might imagine that a phase transition to a superradiant black hole is unphysical — the end state will instead be replaced by the resultant non-superradiant black hole. Note however that the superradiant instabilities were studied in the classical setting (they follow from the instability of the field equations for the class of superradiant Kerr-AdS black holes). It is an interesting question as to whether these can be related to what happens in the thermodynamic ensemble (where for example in the canonical ensemble J is fixed by definition).

We also note that whereas superradiant instabilities are classical, thermodynamic phase transitions are semi-classical. Superradiant instabilities generally set in at much shorter timescales than thermodynamic ones. However it may be that in some circumstances the superradiant phase could be quasi-stable. We have thus included all possible phases (superradiant and non-superradiant). We leave the question of understanding the implications of superradiant phases for (holographic) black hole thermodynamics for future study.

Note added. We note that close to the completion of this project a paper [36] appeared, which has an overlap with our current manuscript. They studied the first two ensembles, but did not consider the novel ensemble in section 3.3.

[3] In the bulk, there are theories in which the cosmological constant Λ can be treated as a dynamical variable [51, 52] but an analogous method that makes C dynamical has, to our knowledge, not been formulated.

JHEP08(2023)142

Acknowledgments

D.K. is grateful for support from GAČ 23-07457S grant of the Czech Science Foundation, as well as would like to acknowledge the kind hospitality of the Perimeter Institute where this work was completed. M.R.V. is supported by SNF Postdoc Mobility grant P500PT-206877 "Semi-classical thermodynamics of black holes and the information paradox". This work was supported in part by the Natural Sciences and Engineering Research Council of Canada. This research was supported in part by Perimeter Institute of Theoretical Physics. Research at Perimeter Institute is supported in part by the Government of Canada through the Department of Innovation, Science and Economic Development and by the Province of Ontario through the Ministry of Colleges and Universities. Perimeter Institute and the University of Waterloo are situated on the Haldimand Tract, land that was promised to the Haudenosaunee of the Six Nations of the Grand River, and is within the territory of the Neutral, Anishnawbe, and Haudenosaunee peoples.

A Grand canonical ensemble in the bulk

The grand canonical ensemble for the bulk rotating black hole system is similar to that of the boundary CFT. We summarise the main features of the bulk grand canonical ensemble in this appendix.

The bulk thermodynamic variables for the Kerr-AdS black hole can be found in the main text. We restate them here for convenience:

$$M = \frac{\Omega_{d-2}}{4\pi G_N}\frac{m}{\Xi^2}\left(1+\frac{(d-4)\Xi}{2}\right), \quad S = \frac{\Omega_{d-2}}{4G}\frac{r_h^{d-4}(a^2+r_h^2)}{\Xi}, \tag{A.1}$$

$$T_H = \frac{1}{2\pi}\left[r_h\left(1+\frac{r_h^2}{L^2}\right)\left(\frac{1}{a^2+r_h^2}+\frac{d-3}{2r_h^2}\right)-\frac{1}{r_h}\right], \tag{A.2}$$

$$\Omega = \frac{a}{L^2}\frac{r_h^2+L^2}{r_h^2+a^2}, \qquad J = \frac{\Omega_{d-2}}{4\pi G_N}\frac{ma}{\Xi^2}, \qquad P = \frac{(d-1)(d-2)}{16\pi G_N L^2}. \tag{A.3}$$

The associated free energy in the grand canonical ensemble is: $W_{\text{bulk}} = M - T_H S - \Omega J$. As in the main text, we study the phase behaviour of the system by looking at the free energy against temperature diagram, plotted in figure 15 for $d = 4$. As in the CFT case, there is a threshold value, $\Omega L = 1$ (cf. $\tilde{\Omega} R = 1$ for the CFT), at which the diagram experiences a qualitative change: for $\Omega L < 1$ the $W_{\text{bulk}} - T_H$ curve displays a Hawking-Page like cusp, while for $\Omega L > 1$ the $W_{\text{bulk}} - T_H$ curve is smooth and positive. For $\Omega L = 1$, the curve is also smooth and positive, but terminates at finite temperature, where $a = L$, beyond which the solution becomes unphysical with $a > L$ (dashed in figure).

As in the CFT case, the behaviour of the rotating black hole in the grand canonical ensemble is somewhat different from that of the charged black hole, illustrated in figure 16 (see also e.g. [6]). In particular, the free energy of the charged system also transitions from a cusp to a smooth curve at some (electric) potential $\Phi = \Phi_c = \sqrt{3}/2$, like in the rotating case. However, unlike the rotating case, the free energy curve with $\Phi \geq \Phi_c$ is *negative* and the "large black hole" phase always dominates over the radiation phase for these values of the potential in the grand canonical ensemble.

JHEP08(2023)142

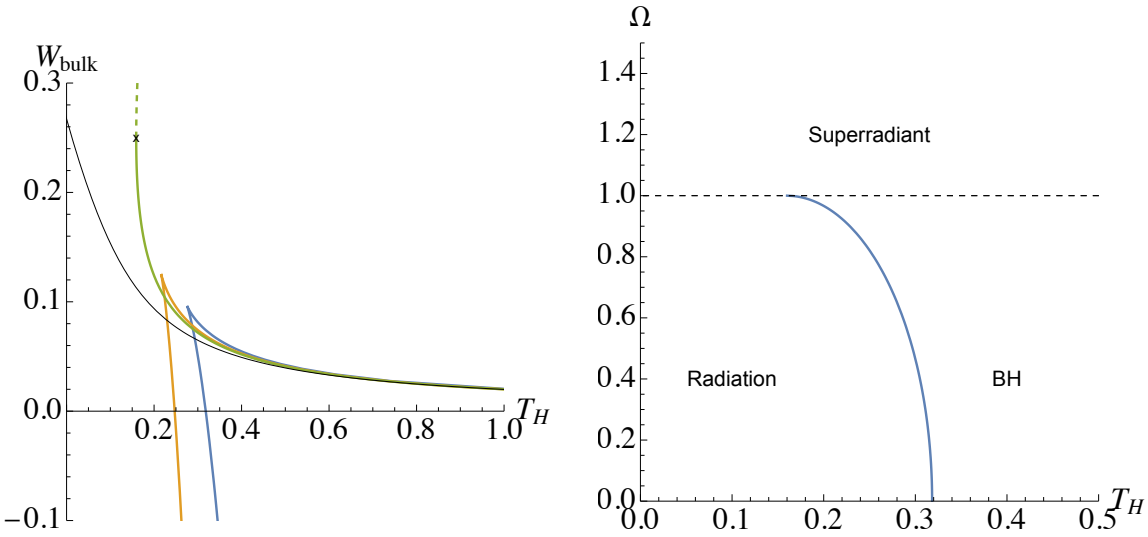

Figure 15. Bulk grand canonical ensemble (at fixed angular velocity Ω) of Kerr-AdS black holes. **Left:** free energy against temperature diagram for $\Omega L = \frac{1}{20}$ (blue), $\Omega L = \frac{5}{6}$ (yellow), $\Omega L = 1$ (green) and $\Omega L = \frac{3}{2}$ (red). The physical part of the $\Omega L = 1$ curve terminates at the point "x", with $a = L$. **Right:** co-existence phase diagram for Ω vs. T_H.

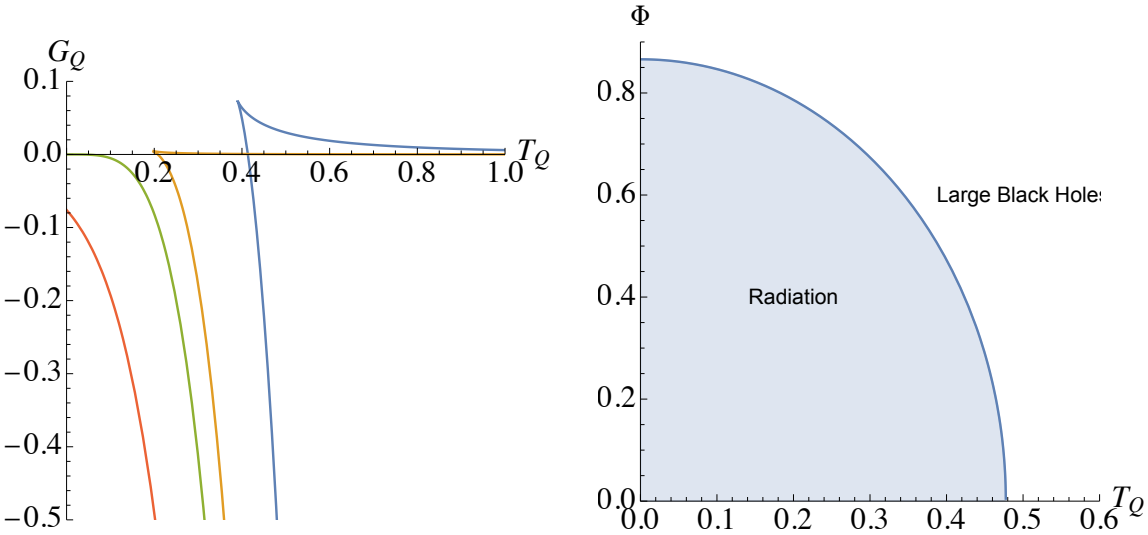

Figure 16. Bulk grand canonical ensemble (at fixed electric potential Φ) of Reissner-Nordström AdS black holes. **Left:** free energy against temperature diagram for $\Phi = 1/2\Phi_c$ (blue), $\Phi = 9/10\Phi_c$ (yellow), $\Phi = \Phi_c = \sqrt{3}/2$ (green) and $\Phi = 6/5\Phi_c$ (red). **Right:** co-existence phase diagram for Φ vs. T_Q.

JHEP08(2023)142

B Phase diagram of fixed $(J, \mathcal{V}, \mu)$ ensemble

In this appendix, we include more details on the $\mu - T$ phase diagrams in figures 10 and 14. As explained in the main text, the phase behaviour of the system is implied by the $G - T$ plots. By studying these in detail, the various zeroth-order phase transition curves on the $d = 4$ phase diagram (figure 10) can be obtained as follows.

1. $\mu > 0$, NS-LE (green): the smallest real root of $G = 0$ (i.e., $x^3 - x + R\mu = 0$), where the free energy G is given by (3.19), is

$$x = \frac{2}{\sqrt{3}} \cos\left(\frac{4\pi}{3} + \frac{1}{3}\cos^{-1}\left(-\frac{3}{2}\sqrt{3}\mu R\right)\right) .$$

   The $T(\mu)$ equation of this zeroth-order phase transition curve can then be obtained directly by substituting this into (3.20).

2. $\mu > 0$, LE-HE and $\mu < 0$, NS-HE (yellow): the second real root of $G = 0$ is

$$x = \frac{\sqrt[3]{2}\left(\sqrt{81\mu^2R^2 - 12} - 9\mu R\right)^{2/3} + 2\sqrt[3]{3}}{6^{2/3}\sqrt[3]{\sqrt{81\mu^2R^2 - 12} - 9\mu R}} ,$$

3. $\mu > 0$, NS-HE (orange): the solution to $\partial G/\partial x|_{\mu,R} = 0$ is given by

$$x = \frac{1}{4}\left(\mu R\left(\frac{\mu R}{\sqrt[3]{\mu^3R^3 + 4\sqrt{\mu^2R^2\left(\mu^2R^2 + 4\right)} + 8\mu R}} + 1\right) + \sqrt[3]{\mu^3R^3 + 4\sqrt{\mu^2R^2\left(\mu^2R^2 + 4\right)} + 8\mu R}\right) .$$

4. The intersection of the above three lines takes place at

$$\mu = \frac{2}{3\sqrt{3}R} , \qquad x = \frac{1}{\sqrt{3}} .$$

5. $\mu > 0$ HE-IE and $\mu < 0$ HE-NS (blue): $z = 1$ point, given by $x = 1$ at which $T = \frac{1}{2\pi R}$.

6. The intersection of the curve in item (3) above with that in item (5) occurs at

$$x = 1 , \qquad \mu = \frac{1}{R} .$$

The $d = 6$ phase diagram (figure 14) can be analysed in an analogous way, but in this case the solutions are mostly roots of polynomials of order ≥ 5 for which no analytic expressions exist. Qualitatively:

1. $\mu > 0$, LE-IE (yellow), $\mu > 0$, IE-HE and $\mu < 0$, NS-HE (orange): these are different solutions to the equation $G(x) = 0$ at given (μ, R).

JHEP08(2023)142

2. $\mu > 0$, IE-NS (blue) and $\mu > 0$, LE-HE (green): these are different solutions to $\partial G/\partial x|_{\mu,R} = 0$.

3. The intersection of the LE-IE and IE-HE transition lines happens at

$$x = \sqrt{\frac{3}{5}}\,, \qquad \mu = \frac{6}{25R}\sqrt{\frac{3}{5}}\,,$$

4. The (purple) vertical line with $z = 1$ occurs at $x = 1$, giving $T = \frac{3}{2\pi R}$.

JHEP08(2023)142

References

[1] J.M. Maldacena, *The Large N limit of superconformal field theories and supergravity*, *Adv. Theor. Math. Phys.* **2** (1998) 231 [hep-th/9711200] [INSPIRE].

[2] E. Witten, *Anti-de Sitter space and holography*, *Adv. Theor. Math. Phys.* **2** (1998) 253 [hep-th/9802150] [INSPIRE].

[3] S.S. Gubser, I.R. Klebanov and A.M. Polyakov, *Gauge theory correlators from noncritical string theory*, *Phys. Lett. B* **428** (1998) 105 [hep-th/9802109] [INSPIRE].

[4] S.W. Hawking and D.N. Page, *Thermodynamics of Black Holes in anti-De Sitter Space*, *Commun. Math. Phys.* **87** (1983) 577 [INSPIRE].

[5] E. Witten, *Anti-de Sitter space, thermal phase transition, and confinement in gauge theories*, *Adv. Theor. Math. Phys.* **2** (1998) 505 [hep-th/9803131] [INSPIRE].

[6] A. Chamblin, R. Emparan, C.V. Johnson and R.C. Myers, *Charged AdS black holes and catastrophic holography*, *Phys. Rev. D* **60** (1999) 064018 [hep-th/9902170] [INSPIRE].

[7] A. Chamblin, R. Emparan, C.V. Johnson and R.C. Myers, *Holography, thermodynamics and fluctuations of charged AdS black holes*, *Phys. Rev. D* **60** (1999) 104026 [hep-th/9904197] [INSPIRE].

[8] M. Cvetic and S.S. Gubser, *Phases of R charged black holes, spinning branes and strongly coupled gauge theories*, *JHEP* **04** (1999) 024 [hep-th/9902195] [INSPIRE].

[9] D. Kubiznak and R.B. Mann, *P-V criticality of charged AdS black holes*, *JHEP* **07** (2012) 033 [arXiv:1205.0559] [INSPIRE].

[10] B.P. Dolan, A. Kostouki, D. Kubiznak and R.B. Mann, *Isolated critical point from Lovelock gravity*, *Class. Quant. Grav.* **31** (2014) 242001 [arXiv:1407.4783] [INSPIRE].

[11] N. Altamirano, D. Kubiznak and R.B. Mann, *Reentrant phase transitions in rotating anti–de Sitter black holes*, *Phys. Rev. D* **88** (2013) 101502 [arXiv:1306.5756] [INSPIRE].

[12] A.M. Frassino, D. Kubiznak, R.B. Mann and F. Simovic, *Multiple Reentrant Phase Transitions and Triple Points in Lovelock Thermodynamics*, *JHEP* **09** (2014) 080 [arXiv:1406.7015] [INSPIRE].

[13] N. Altamirano, D. Kubizňák, R.B. Mann and Z. Sherkatghanad, *Kerr-AdS analogue of triple point and solid/liquid/gas phase transition*, *Class. Quant. Grav.* **31** (2014) 042001 [arXiv:1308.2672] [INSPIRE].

[14] S.-W. Wei and Y.-X. Liu, *Triple points and phase diagrams in the extended phase space of charged Gauss-Bonnet black holes in AdS space*, *Phys. Rev. D* **90** (2014) 044057 [arXiv:1402.2837] [INSPIRE].

[15] R.A. Hennigar, R.B. Mann and E. Tjoa, *Superfluid Black Holes*, *Phys. Rev. Lett.* **118** (2017) 021301 [arXiv:1609.02564] [INSPIRE].

[16] M. Tavakoli, J. Wu and R.B. Mann, *Multi-critical points in black hole phase transitions*, *JHEP* **12** (2022) 117 [arXiv:2207.03505] [INSPIRE].

[17] J. Wu and R.B. Mann, *Multicritical phase transitions in multiply rotating black holes*, *Class. Quant. Grav.* **40** (2023) 06LT01 [arXiv:2208.00012] [INSPIRE].

[18] D. Kastor, S. Ray and J. Traschen, *Enthalpy and the Mechanics of AdS Black Holes*, *Class. Quant. Grav.* **26** (2009) 195011 [arXiv:0904.2765] [INSPIRE].

[19] B.P. Dolan, *Pressure and volume in the first law of black hole thermodynamics*, *Class. Quant. Grav.* **28** (2011) 235017 [arXiv:1106.6260] [INSPIRE].

[20] B.P. Dolan, *The cosmological constant and the black hole equation of state*, *Class. Quant. Grav.* **28** (2011) 125020 [arXiv:1008.5023] [INSPIRE].

[21] M. Cvetic, G.W. Gibbons, D. Kubiznak and C.N. Pope, *Black Hole Enthalpy and an Entropy Inequality for the Thermodynamic Volume*, *Phys. Rev. D* **84** (2011) 024037 [arXiv:1012.2888] [INSPIRE].

[22] D. Kubiznak and R.B. Mann, *Black hole chemistry*, *Can. J. Phys.* **93** (2015) 999 [arXiv:1404.2126] [INSPIRE].

[23] D. Kubiznak, R.B. Mann and M. Teo, *Black hole chemistry: thermodynamics with Lambda*, *Class. Quant. Grav.* **34** (2017) 063001 [arXiv:1608.06147] [INSPIRE].

[24] G.W. Gibbons, M.J. Perry and C.N. Pope, *The First law of thermodynamics for Kerr-anti-de Sitter black holes*, *Class. Quant. Grav.* **22** (2005) 1503 [hep-th/0408217] [INSPIRE].

[25] M.B. Ahmed et al., *Holographic Dual of Extended Black Hole Thermodynamics*, *Phys. Rev. Lett.* **130** (2023) 181401 [arXiv:2302.08163] [INSPIRE].

[26] A. Karch and B. Robinson, *Holographic Black Hole Chemistry*, *JHEP* **12** (2015) 073 [arXiv:1510.02472] [INSPIRE].

[27] M.R. Visser, *Holographic thermodynamics requires a chemical potential for color*, *Phys. Rev. D* **105** (2022) 106014 [arXiv:2101.04145] [INSPIRE].

[28] W. Cong, D. Kubiznak and R.B. Mann, *Thermodynamics of AdS Black Holes: Critical Behavior of the Central Charge*, *Phys. Rev. Lett.* **127** (2021) 091301 [arXiv:2105.02223] [INSPIRE].

[29] G. Zeyuan and L. Zhao, *Restricted phase space thermodynamics for AdS black holes via holography*, *Class. Quant. Grav.* **39** (2022) 075019 [arXiv:2112.02386] [INSPIRE].

[30] T. Wang and L. Zhao, *Black hole thermodynamics is extensive with variable Newton constant*, *Phys. Lett. B* **827** (2022) 136935 [arXiv:2112.11236] [INSPIRE].

[31] I.P. Lobo, J.P. Morais Graça, E. Folco Capossoli and H. Boschi-Filho, *A varying gravitational constant map in asymptotically AdS black hole thermodynamics*, *Phys. Lett. B* **835** (2022) 137559 [arXiv:2206.13664] [INSPIRE].

[32] W. Cong, D. Kubiznak, R.B. Mann and M.R. Visser, *Holographic CFT phase transitions and criticality for charged AdS black holes*, *JHEP* **08** (2022) 174 [arXiv:2112.14848] [INSPIRE].

[33] Z. Gao, X. Kong and L. Zhao, *Thermodynamics of Kerr-AdS black holes in the restricted phase space*, *Eur. Phys. J. C* **82** (2022) 112 [arXiv:2112.08672] [INSPIRE].

JHEP08(2023)142

[34] L. Zhao, *Thermodynamics for higher dimensional rotating black holes with variable Newton constant*, *Chin. Phys. C* **46** (2022) 055105 [arXiv:2201.00521] [INSPIRE].

[35] X. Kong, T. Wang, Z. Gao and L. Zhao, *Restricted Phased Space Thermodynamics for Black Holes in Higher Dimensions and Higher Curvature Gravities*, *Entropy* **24** (2022) 1131 [arXiv:2208.07748] [INSPIRE].

[36] T.-F. Gong, J. Jiang and M. Zhang, *Holographic thermodynamics of rotating black holes*, *JHEP* **06** (2023) 105 [arXiv:2305.00267] [INSPIRE].

[37] D. Kastor, S. Ray and J. Traschen, *Smarr Formula and an Extended First Law for Lovelock Gravity*, *Class. Quant. Grav.* **27** (2010) 235014 [arXiv:1005.5053] [INSPIRE].

[38] D. Kastor, S. Ray and J. Traschen, *Chemical Potential in the First Law for Holographic Entanglement Entropy*, *JHEP* **11** (2014) 120 [arXiv:1409.3521] [INSPIRE].

[39] D. Sarkar and M. Visser, *The first law of differential entropy and holographic complexity*, *JHEP* **11** (2020) 004 [arXiv:2008.12673] [INSPIRE].

[40] B. Carter, *Hamilton-Jacobi and Schrodinger separable solutions of Einstein's equations*, *Commun. Math. Phys.* **10** (1968) 280 [INSPIRE].

[41] S.W. Hawking, C.J. Hunter and M. Taylor, *Rotation and the AdS / CFT correspondence*, *Phys. Rev. D* **59** (1999) 064005 [hep-th/9811056] [INSPIRE].

[42] G.W. Gibbons, H. Lu, D.N. Page and C.N. Pope, *The General Kerr-de Sitter metrics in all dimensions*, *J. Geom. Phys.* **53** (2005) 49 [hep-th/0404008] [INSPIRE].

[43] G.W. Gibbons, H. Lu, D.N. Page and C.N. Pope, *Rotating black holes in higher dimensions with a cosmological constant*, *Phys. Rev. Lett.* **93** (2004) 171102 [hep-th/0409155] [INSPIRE].

[44] T. Jacobson and M. Visser, *Gravitational Thermodynamics of Causal Diamonds in (A)dS*, *SciPost Phys.* **7** (2019) 079 [arXiv:1812.01596] [INSPIRE].

[45] G.W. Gibbons, M.J. Perry and C.N. Pope, *AdS/CFT Casimir energy for rotating black holes*, *Phys. Rev. Lett.* **95** (2005) 231601 [hep-th/0507034] [INSPIRE].

[46] V. Cardoso, O.J.C. Dias and S. Yoshida, *Classical instability of Kerr-AdS black holes and the issue of final state*, *Phys. Rev. D* **74** (2006) 044008 [hep-th/0607162] [INSPIRE].

[47] S.W. Hawking and H.S. Reall, *Charged and rotating AdS black holes and their CFT duals*, *Phys. Rev. D* **61** (2000) 024014 [hep-th/9908109] [INSPIRE].

[48] S. Gunasekaran, R.B. Mann and D. Kubiznak, *Extended phase space thermodynamics for charged and rotating black holes and Born-Infeld vacuum polarization*, *JHEP* **11** (2012) 110 [arXiv:1208.6251] [INSPIRE].

[49] S. Kim et al., *'Grey Galaxies' as an endpoint of the Kerr-AdS superradiant instability*, arXiv:2305.08922 [INSPIRE].

[50] N. Altamirano, D. Kubiznak, R.B. Mann and Z. Sherkatghanad, *Thermodynamics of rotating black holes and black rings: phase transitions and thermodynamic volume*, *Galaxies* **2** (2014) 89 [arXiv:1401.2586] [INSPIRE].

[51] M. Henneaux and C. Teitelboim, *The cosmological constant as a canonical variable*, *Phys. Lett. B* **143** (1984) 415 [INSPIRE].

[52] C. Teitelboim, *The cosmological constant as a thermodynamic black hole parameter*, *Phys. Lett. B* **158** (1985) 293 [INSPIRE].

[53] P. De Lange, A. Maloney and E. Verlinde, *Monstrous Product CFTs in the Grand Canonical Ensemble*, arXiv:1807.06200 [INSPIRE].

JHEP08(2023)142